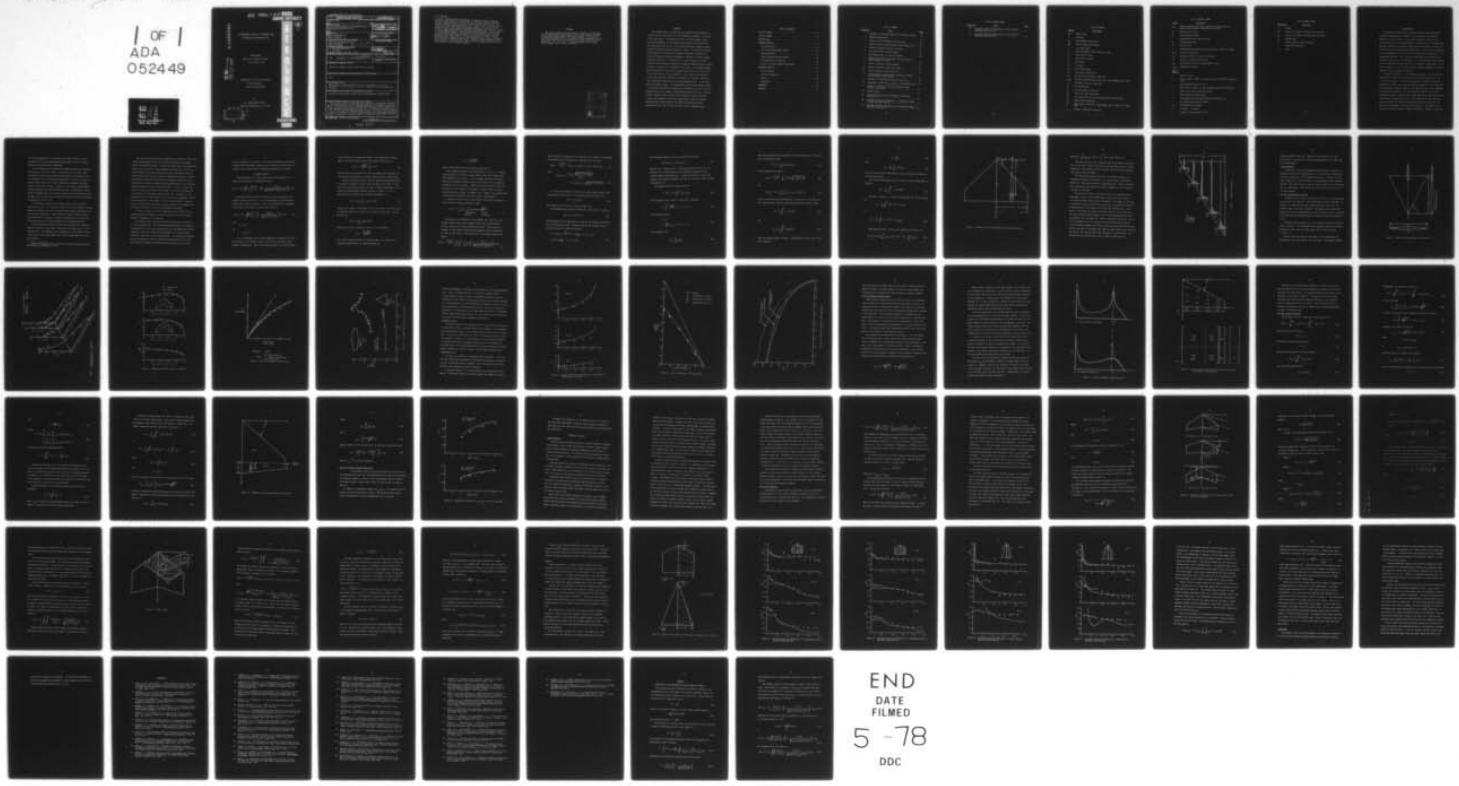
AD-A052 449 AUBURN UNIV ALA ENGINEERING EXPERIMENT STATION F/G 20/4
AN AERODYNAMIC ANALYSIS OF DEFORMED WINGS IN SUBSONIC AND SUPER--ETC(U)
MAR 78 J E BURKHALTER, J W PURVIS DAAG29-77-G-0069
UNCLASSIFIED ARO-14802.1-A-E NL

1 OF 1
ADA
052449



END
DATE
FILMED
5-78
DDC

ARO 14802.1-A-E

AUBURN UNIVERSITY

AERONAUTICAL ENGINEERING

(10)

AD A052449

AN AERODYNAMIC ANALYSIS OF DEFORMED WINGS IN SUBSONIC AND SUPERSONIC FLOW

FINAL REPORT

Contract No. DAAG29-77-G-0069

Jan. 1977-Dec. 1977

AD No.
DDC FILE COPY

Department of Aerospace Engineering

Auburn University

Auburn, Alabama 36830

for

U.S. Army Research Office

Research Triangle Park, N.C. 27709

DDC
RECEIVED
APR 4 1978
E

UNCLASSIFIED

SECURITY CLASSIFICATION OF THIS PAGE (When Data Entered)

REPORT DOCUMENTATION PAGE

READ INSTRUCTIONS BEFORE COMPLETING FORM

1. REPORT NUMBER

2. GOVT ACCESSION NO.

3. RECIPIENT'S CATALOG NUMBER

4. TITLE (and Subtitle)

An Aerodynamic Analysis of Deformed Wings in Subsonic and Supersonic Flow

5. TYPE OF REPORT & PERIOD COVERED

Final Report
Jan[redacted]-Dece[redacted]977,

6. PERFORMING ORG. REPORT NUMBER

7. AUTHOR(s)

John E. Burkhalter
James W. Purvis

8. CONTRACT OR GRANT NUMBER(s)

DAAG29-77-G-0069

9. PERFORMING ORGANIZATION NAME AND ADDRESS

Engineering Experiment Station
Auburn University
Auburn, AL 36830

402 958

10. PROGRAM ELEMENT, PROJECT, TASK AREA & WORK UNIT NUMBERS

11. CONTROLLING OFFICE NAME AND ADDRESS

U. S. Army Research Office
P. O. Box 12211
Research Triangle Park, NC 27709

12. REPORT DATE

Mar[redacted]978

13. NUMBER OF PAGES

~~74~~ 76

14. MONITORING AGENCY NAME & ADDRESS(if different from Controlling Office)

Same

ARO

14802.1-A-E

15. SECURITY CLASS. (of this report)

unclassified

15a. DECLASSIFICATION/DOWNGRADING SCHEDULE

16. DISTRIBUTION STATEMENT (of this Report)

Approved for public release; distribution unlimited.

17. DISTRIBUTION STATEMENT (of the abstract entered in Block 20, if different from Report)

Same

18. SUPPLEMENTARY NOTES

The findings in this report are not to be construed as an official Department of the Army position, unless so designated by other authorized documents.

19. KEY WORDS (Continue on reverse side if necessary and identify by block number)

Aerodynamic Wing Loading, Elevon Loading, Hinge Moments, Deformed Wings

20. ABSTRACT (Continue on reverse side if necessary and identify by block number)

The research effort for the past year involved the development of theoretical prediction methods for the aerodynamic loading on a wing with a full span elevon. The methods are based on lifting surface kernel function formulations in both subsonic and supersonic potential flow. The unique idea in both cases is the closed form-finite summation manner in which the kernel function integral is solved. This method of solution avoides Mangler- and Cauchy-type singularity problems, encountered in classical numerical integration approaches, and leads

Over

DD FORM 1 JAN 73 1473 EDITION OF 1 NOV 65 IS OBSOLETE

Unclassified

SECURITY CLASSIFICATION OF THIS PAGE (When Data Entered)

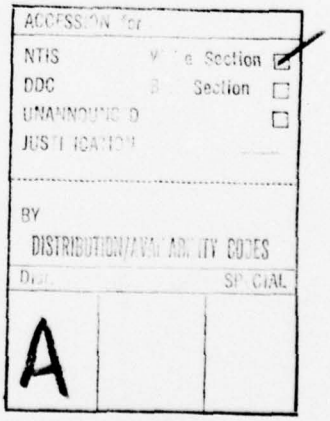
JOB 402 958

20 (Continued)

to stable, rapidly convergent solutions. In subsonic flow, an existing kernel function method for planar wings was modified by adding an assumed pressure loading function to account for the presence of the elevon. The assumed pressure loading distribution led to exact closed form solutions for section and total coefficients on the wing; however, for the case of the deflected elevon, some numerical integration procedures were required. Results of these computations agree very well with experimental data. In the supersonic Mach number regime, a lifting surface kernel function method similar to the subsonic approach was developed for the planar wing case, but with appropriate Mach cone regions of integration taken into account. Various assumed pressure loading functions, all weighted by exact theoretical results, were required for different wing shapes. Numerical results produced stable (nonoscillatory) solutions which agreed well with experimental data, even for very low aspect ratio triangular wings.

PREFACE

The work as reported in this document represents the completion of the various tasks as prescribed in Contract No. DAAG29-77-G-0069, for the Army Missile Command, Huntsville, Alabama. The research is monitored through the U.S. Army Research Office, Research Triangle Park, North Carolina and is the result of the work done during the period Jan. 1977 - Dec. 1977. The program manager with the Army Missile Command was Dr. Donald J. Spring.



SUMMARY

The research effort for the past year involved the development of theoretical prediction methods for the aerodynamic loading on a wing with a full span elevon. The methods are based on lifting surface kernel function formulations in both subsonic and supersonic potential flow. The unique idea in both cases is the closed form-finite summation manner in which the kernel function integral is solved. This method of solution avoids Mangler- and Cauchy-type singularity problems, encountered in classical numerical integration approaches, and leads to stable, rapidly convergent solutions. In subsonic flow, an existing kernel function method for planar wings was modified by adding an assumed pressure loading function to account for the presence of the elevon. The assumed pressure loading distribution led to exact closed form solutions for section and total coefficients on the wing; however, for the case of the deflected elevon, some numerical integration procedures were required. Results of these computations agree very well with experimental data. In the supersonic Mach number regime, a lifting surface kernel function method similar to the subsonic approach was developed for the planar wing case, but with appropriate Mach cone regions of integration taken into account. Various assumed pressure loading functions, all weighted by exact theoretical results, were required for different wing shapes. Numerical results produced stable (nonoscillatory) solutions which agreed well with experimental data, even for very low aspect ratio triangular wings.

TABLE OF CONTENTS

LIST OF FIGURES ii

LIST OF SYMBOLS iv

INTRODUCTION 1

SUBSONIC ANALYSIS 4

ΔC_p Distribution 14

Lift and Pitching Moment Results 14

Thickness Effects 20

Elevon Loading and Hinge Moments 24

Sectional Loads and Moments. 28

Results of Elevon Loading Computations 33

SUPERSONIC ANALYSIS 35

Current Methods 35

Theoretical Approach 37

Results. 49

Conclusions 56

REFERENCES 59

APPENDIX 64

LIST OF FIGURES

Figure No.	Title	Page
1	Schematic of the Wing Geometry and Coordinate System.	11
2	Downwash Distribution	13
3	Sketch of Thick Wing Model (Reference 38)	15
4	Planform Pressure Distribution on Delta Wing (M_∞=.13)	16
5	Spanwise Loading and Center of Pressure	17
6	Lift Curve Slopes for Delta Wings	18
7	Mach Number Effect on Lift Curve Slopes	19
8	Spanwise Variation of Sectional Lift Coefficient at Various Angles of Attack.	21
9	Center of Pressure on Wing Planform	22
10	Spanwise Loading for Thick Wing (Wick).	23
11	Typical Chordwise Loading Functions	26
12	Typical Control Point Locations and Matrix Schematic for Wing-Elevon Configuration	27
13	Schematic for Coordinate System for the Elevon.	32
14	Aerodynamic Coefficient C_{L_α} and C_{L_δ} versus Aspect Ratio	34
15	Regions of Integration for the Supersonic Kernel Function Formulation.	41
16	Element Shapes.	45
17	Control Point Location on Two Wings in Supersonic Flow (Ref. 42).	50
18	Chordwise Pressure Distribution on a Trapezoidal Wing in Supersonic Flow (M=1.61)	51
19	Chordwise Pressure Distribution on a Trapezoidal Wing in Supersonic Flow (M=2.1)	52

LIST OF FIGURES (CONT)

Figure No.	Title	Page
20	Chordwise Pressure Distribution on a Delta Wing in Supersonic Flow (M=1.61)	53
21	Chordwise Pressure Distribution on a Delta Wing in Supersonic Flow (M=2.01)	54

LIST OF SYMBOLS

Symbol	Definition
AR	Aspect ratio
b	Wing span
B_{nm}	Wing loading coefficients
B_{pq}	Elevon loading coefficients
c	Local wing chord
$\bar{c}$	Mean aerodynamic chord, reference length
c_w	Local chord of wing
c_E	Local chord of elevon
c_R	Root chord
c_T	Tip chord
c_{To}	Total chord length
cc_ℓ	Section lift coefficient
cc_m	Section pitching moment coefficient
cc_{mrc}	Sectional pitching moment about root chord leading edge (y axis)
c_{ℓ_α}	Sectional lift curve slope (α=0)
C_L	Lift coefficient
C_m	Pitching moment coefficient
C_{L_α}	Total lift curve slope (α=0)
C_{L_δ}	Lift curve slope due to elevator deflection (α=0)($dC_L/d\delta$)
C_{D_i}	Induced drag coefficient
C_H	Hinge moment coefficient = $M_{HL}/(qs_E\bar{c}_E)$, M_{HL} = moment about hinge line
C_p	Pressure coefficient, $(p-p_\infty)/q_\infty$

Symbol	Definition
ΔC_p	Pressure loading coefficient, difference between upper and lower surface pressure coefficients at a point
HL	Hinge line of elevon
M_∞	Freestream Mach number
S	Wing planform area, reference area
V_∞	Freestream velocity
$\vec{V}$	Vector vector
w	Non-dimensional perturbation velocity W/V_∞, parallel to z-axis
x,y,z	Cartesian coordinates
x_{cp}	Chordwise location of center of pressure
x_H	Hinge line location along x axis
x_{LE}	Distance from y-axis to leading edge of wing
x_o, y_o	Integration variables
Greek Symbols	
α	Angle of attack
β	Mach parameter, $\sqrt{1-M_\infty^2}$ for subsonic flow and $\sqrt{M_\infty^2-1}$ for supersonic flow
γ	Non-dimensional vorticity Γ/V_∞
δ	Elevon angle relative to wing (trailing edge down is positive)
λ	Taper ratio, (tip chord)/(root chord)
Λ	Wing leading edge sweep angle
ϕ	Non-dimensional perturbation velocity potential ϕ/V_∞
θ	Non-dimensional spanwise variable
ξ,η	Non-dimensional variables
π	3.1415927..., constant
σ	Tangent of LE sweep angle = tan Λ

Subscripts	Definition
E	Elevon
nm	Points or constants associated with the wing
pq	Points or constants associated with the elevon
LE	Leading edge
o	Denotes wing coordinate variables
∞	Freestream conditions
W	Wing

INTRODUCTION

The problem of predicting the wing and control surface loading and associated hinge moments of a missile in both subsonic and supersonic flight has been the subject of the present research for the last year (since January 1977). More specifically, the loading for a "deformed wing" has been studied and preliminary results have been obtained. Problems of this nature have been extensively studied (Refs. 1-35) and can be approached in three fundamental ways. The first and perhaps the most expensive is the experimental approach. Wind tunnel tests have been used extensively for problems of this nature for many years. For obvious reasons, this procedure is rather expensive and long lead times are required. Additionally, extension of the data to other configurations is somewhat questionable and can sometimes lead to erroneous conclusions.

The second approach is a finite element approach. The flow field is subdivided into small finite elements and the field properties are computed at each element. For most real problems, the element size must be significantly smaller than some characteristic dimension of the flow field and consequently elements numbering in the thousands and tens of thousands are generally required even for two-dimensional analyses. For three-dimensional problems, another order of magnitude must be added which would require very long computer run times. The advantages of such approaches are good accuracy and usually good detailed information concerning the flow field, aerodynamic loads and field properties. The scheme is not limited to inviscid flow nor to small perturbations. However, it was felt

that the disadvantages of long computer run times, high cost, and restriction for full three-dimensional flows prohibit the use of finite element or finite difference approaches.

The third approach is fundamentally founded in linearized potential flow theory and is the one taken in the present research work. Many techniques for solving the potential flow problem are available and two are basically used in wing loading computations. The first is based on vortex lattice theory and is used extensively for problems concerning wings and other lifting bodies. However, it too requires large computer storage (normally) and relatively long run times. Additionally, vortex lattice techniques fail to accurately predict the wing loading near trailing edges (Ref. 37) and tend to produce oscillatory pressure distributions in supersonic flow (Ref. 31).

For the present research, the lifting surface (kernel function) formulation is used. This approach is known to give good agreement between theory and experiment but past formulations have required integration over a second order singularity. This problem has, however, been overcome in the present work by removing the pressure loading term in the equations which allows direct closed form integration of the remaining terms.

The coding described above has been used to determine the loading on wings and elevons and hinge moment calculations have been made for these configurations. The analysis is also applicable to the "detached" elevon case in which a gap* exists between the elevon leading edge and the wing trailing edge.

---

*Under the assumption that the gap is less than local wing chord and wing wake has no significant rollup.

The use of the kernel function formulation as described in this report retains the advantages of the theory while eliminating or minimizing some of its inherent problems. Lifting line, thin airfoil and slender wing theory results are used to develop general functional forms for the ΔC_p distributions and the basic integral equation is expressed in terms of vorticity which satisfies the linearized compressible potential equation. The functional forms for the spanwise and chordwise loadings are by no means based on empirical results from experimental data but are logically deduced from exact theories as mentioned above. In fact, the thin airfoil and lifting line theories can be shown to be special limiting cases of the general lifting surface integral (Ref. 34). Evaluation of the integral results are very similar to the vortex lattice equations. Use of the Multhopp spacing (for subsonic flow) for control points in subsonic flow, in conjunction with the above, produces accurate flow tangency over the entire wing without the use of least-squares formulation.

In order to provide a complete formulation of the problem (in one document) the basic elements of the entire derivation of the potential equation is presented in the Appendix.

For supersonic flow, the basic approach uses potential flow theory as in the subsonic case. This allows the general problem to be modeled as a superposition of the various singularities with the appropriate boundary conditions. There is an additional requirement that the flow remain attached at every point on the lifting surface. The pressure distribution on the wing surface is found by solving the supersonic kernel function, which relates the pressure distribution over the surface to the local

surface velocities. The details of the theory and numerical method will be given in the Supersonic Analysis section following a brief review of various current methods used in supersonic potential flow problems.

SUBSONIC ANALYSIS

From the Appendix it is shown that the potential equation for a planar lifting surface in compressible flow is

$$\phi(x,y,z) = \frac{1}{4\pi} \iint_S \frac{\gamma(x_o,y_o)}{(y-y_o)^2 + z^2} \; z \left[1 + \frac{(x-x_o)}{\sqrt{(x-x_o)^2+\beta^2 \; (y-y_o)^2+\beta^2 z^2}} \right] dx_o \; dy_o$$

Using the relation between the surface vorticity strength and the pressure loading coefficient $\gamma = \Delta C_p/2$ and employing the dimensionless spanwise and chordwise variables η and ξ, the nondimensional normalwash in the plane of the sheet due to the sheet itself is

$$w(x,y) = \frac{1}{8\pi} \iint_S \frac{\Delta C_p(\xi,\eta)}{(y-y_o)^2} \left[1 + \frac{(x-x_o)}{\sqrt{(x-x_o)^2+\beta^2 (y-y_o)^2}} \right] dx_o \; dy_o \qquad (2)$$

where

$$\eta = y/(b/2)$$

and

$$\xi = (x-x_{LE})/c(\eta)$$

If ΔC_p is expressed as the proper combination of spanwise and chordwise variables, the behavior along a chord or across the span can be examined independently. Since the loading along each chord should behave

in the classical two-dimensional manner at the leading and trailing edges, thin airfoil theory results can be used to define ΔC_p as

$$\Delta C_p(\xi,\eta) = \sqrt{\frac{1-\xi}{\xi}} \sum_{n=0}^{N} A_n(\eta)\xi^n \quad . \tag{3}$$

The first term (n=0) produces the required leading edge singularity (at ξ=0) and each term satisfies the Kutta condition at the trailing edge.

Lifting line theory indicates that the spanwise coefficients should be elliptic in nature for finite values of taper ratio, while for zero taper ratio the required behavior is that of slender wing theory. Introducing the nondimensional spanwise variable, θ, where $\eta = \cos\theta$, a functional form satisfying both of these requirements is

$$A_n(\eta) = \frac{1}{c(\eta)} \sum_{m=0}^{M} B_{nm} \sin(2m+1)\theta \tag{4}$$

The B_{nm}'s are constant coefficients and the $c(\eta)$ term is the local chord. To check the validity of Equation (4), consider a delta wing. For m=0, we then have

$$A_n(\eta) = \frac{1}{c_R(1-\eta)} [B_{n1} \sin\theta] \ .$$

However, $\sin\theta$ may be written as, $\sin\theta = \sqrt{1-\eta^2}$, and hence

$$A_n(\eta) = \frac{B_{n1}}{c_R}\sqrt{\frac{1+\eta}{1-\eta}}$$

which is the required behavior for slender wings. For the case of a straight nontapered wing, the m=0 term reduces to

$$A_n(\eta) = \frac{B_{n1}}{c_R}\sqrt{1-\eta^2}$$

which is the required elliptic spanwise loading term.

Other terms in Equation (4) corresponding to m = 1,2,3,..., merely form corrections of a Fourier Series nature to the basic elliptic term which dominates the solution. It may be argued that other functional forms for the spanwise loading could be used and that the one presented in Equation (4) is not unique. Indeed this is true and other forms have been used but the trigometric functional sin $(2m+1)\theta$ seems to produce the better results at least for subsonic flow. However, any solution which is used must be dominated by the basic elliptic loading terms.

If Equations (3) and (4) are now combined, the complete expression for the pressure loading coefficient becomes

$$\Delta C_p(\xi,\eta) = \sum_{n=0}^{N} \frac{1}{c(\eta)} \underbrace{\sum_{m=0}^{M} B_{nm} \sin(2m+1)\theta}_{\text{Spanwise}} \underbrace{\sqrt{\frac{1-\xi}{\xi}}\,\xi^n}_{\text{Chordwise}} \tag{5}$$

Returning to the evaluation of the downwash, note that over a sufficiently small element of the planform surface ΔC_p is approximately constant, and so can be taken outside the integral. This procedure is analogous to the constant panel loading assumption which is fundamental to vortex lattice theory. The downwash due to this small element then becomes

$$\Delta w(x,y) = \frac{\Delta C_p(\bar{\xi},\bar{\eta})}{8\pi} \int_{y_1}^{y_2}\int_{x_1}^{x_2} \frac{1}{(y-y_o)^2}\left(1 + \frac{(x-x_o)}{\sqrt{(x-x_o)^2+\beta^2\,(y-y_o)^2}}\right) dx_o\, dy_o \tag{6}$$

where $\Delta C_p(\bar{\xi},\bar{\eta})$ is evaluated at the centroid of the element. The integral thus obtained can be evaluated in closed form with the result

$$\Delta w(x,y) = \frac{\Delta C_p(\bar{\xi},\bar{\eta})}{8\pi} \left[K(x_2,y_2) - K(x_2,y_1) - K(x_1,y_2) + K(x_1,y_1)\right] \tag{7}$$

where

$$K(x_o,y_o) = -\frac{(x-x_o) + \sqrt{(x-x_o)^2 + \beta^2(y-y_o)^2}}{(y-y_o)}$$

$$+ \beta \log_e\left[\beta(y-y_o) + \sqrt{(x-x_o)^2 + \beta^2(y-y_o)^2}\right] \tag{8}$$

If the entire planform is divided into similar small elements, the total downwash at any point on the wing surface may be written as

$$w(x,y) = \sum_S \Delta w(x,y) \tag{9}$$

where Equations (5) and (7) are used to evaluate Δw.

The nondimensional tangency condition for small angles of attack is

$$w(x,y) + \sin \alpha(x,y) = 0 \tag{10}$$

which defines the load distribution in terms of the physical requirements of no flow through the wing. Choosing spanwise and chordwise control points according to a cosine distribution

$$x_i = x_{LE}(y_j) + \frac{c(y_j)}{2}\left(1 - \cos\frac{\pi i}{N+1}\right), \quad i = 1,2,\ldots N+1$$

$$y_j = \frac{b}{2}\cos\frac{\pi j}{2M+2}, \quad j = 1,2,\ldots M+1 \tag{11}$$

and evaluating Equation (10) at each control point gives:

$$\sum_{S} \Delta w(x_i,y_j) + \sin \alpha(x_i,y_j) = 0 \tag{12}$$

Equation (12), together with the defining relations (5) and (7), constitutes a set of simultaneous linear algebraic equations for NxM unknown loading coefficients B_{nm}. Solving the system for these coefficients, the pressure loading at any point on the wing is then available from Equation (5).

The spanwise section loading is given by

$$cc_{\ell}(y_o) = c(y_o) \int_0^1 \Delta C_p(\xi,\eta_o) d\xi \tag{13}$$

This integration can be done in closed form. Defining

$$I_n = \int_0^1 \xi^n \sqrt{\frac{1-\xi}{\xi}}\, d \quad , n = 0,1,\ldots,N \tag{14}$$

and integrating yields

$$\begin{aligned} I_o &= \frac{\pi}{2} \\ I_n &= \frac{2n-1}{2n+2} \; I_{n-1} \quad , n = 1,2,\ldots,N \end{aligned} \tag{15}$$

For convenience, let

$$E_m = \sum_{n=0}^{N} B_{nm} I_n \tag{16}$$

then after substitution into Equation (13) from Equations (7), (15) and (16), successively yields

$$cc_{\ell}(y_o) = \sum_{m=0}^{M} E_m \sin(2m+1)\theta \ . \tag{17}$$

Similar manipulations lead to

$$cc_d(y_o) = \frac{cc_{\ell}(y_o)}{8} \sum_{M=0}^{M} (2m+1)E_m \left[\frac{\sin(2m+1)\theta_o}{\sin \theta_o}\right] \tag{18}$$

and

$$cc_m(y_o) = -c(y_o) \sum_{m=0}^{M} \sum_{n=0}^{N} B_{nm} I_{n+1} \sin(2m+1)\theta_o \tag{19}$$

for the section drag and pitching moment, respectively. The total lift and induced drag are found by evaluating the standard integral forms

$$C_L = \frac{1}{S} \int_{-b/2}^{b/2} cc_{\ell}(y_o)dy_o \tag{20}$$

and

$$C_{D_i} = \frac{1}{S} \int_{-b/2}^{b/2} cc_d(y_o)dy_o \tag{21}$$

Using the spanwise angular variable θ and Equations (17) and (18) in the above results in

$$C_L = \frac{\pi E_o}{2S} \tag{22}$$

and

$$C_{D_i} = \frac{\pi}{16S} \sum_{m=0}^{M} (2m+1) E_m^{\,2} \tag{23}$$

which are the classical forms similar to those obtained from Glauert's lifting line analysis.

The total pitching moment about the wing root chord leading edge is found by

$$C_m = -\frac{1}{S\bar{c}} \int_{-b/2}^{b/2} cc_\ell(y)\bar{x}(y)dy \tag{24}$$

Referring to Figure 1, it is seen that Equation (24) may be written as

$$C_m = -\frac{2}{S\bar{c}} \int_0^{\frac{1}{2}} cc_\ell(y \tan \Lambda + x_{cp})dy$$

or

$$C_m = -\frac{2}{S\bar{c}} \int_0^1 (cc_\ell\, y \tan \Lambda + cc_{m_{LE}})dy \tag{25}$$

Using Equations (16), (17) and (18), Equation (25) results in

$$C_m = \frac{1}{S\bar{c}} \left[(c_R - c_T) \sum_{m=0}^{M} F_m G_m - \frac{\pi}{2} c_R F(1) - \tan \Lambda \sum_{m=0}^{M} E_m G_m\right] \tag{26}$$

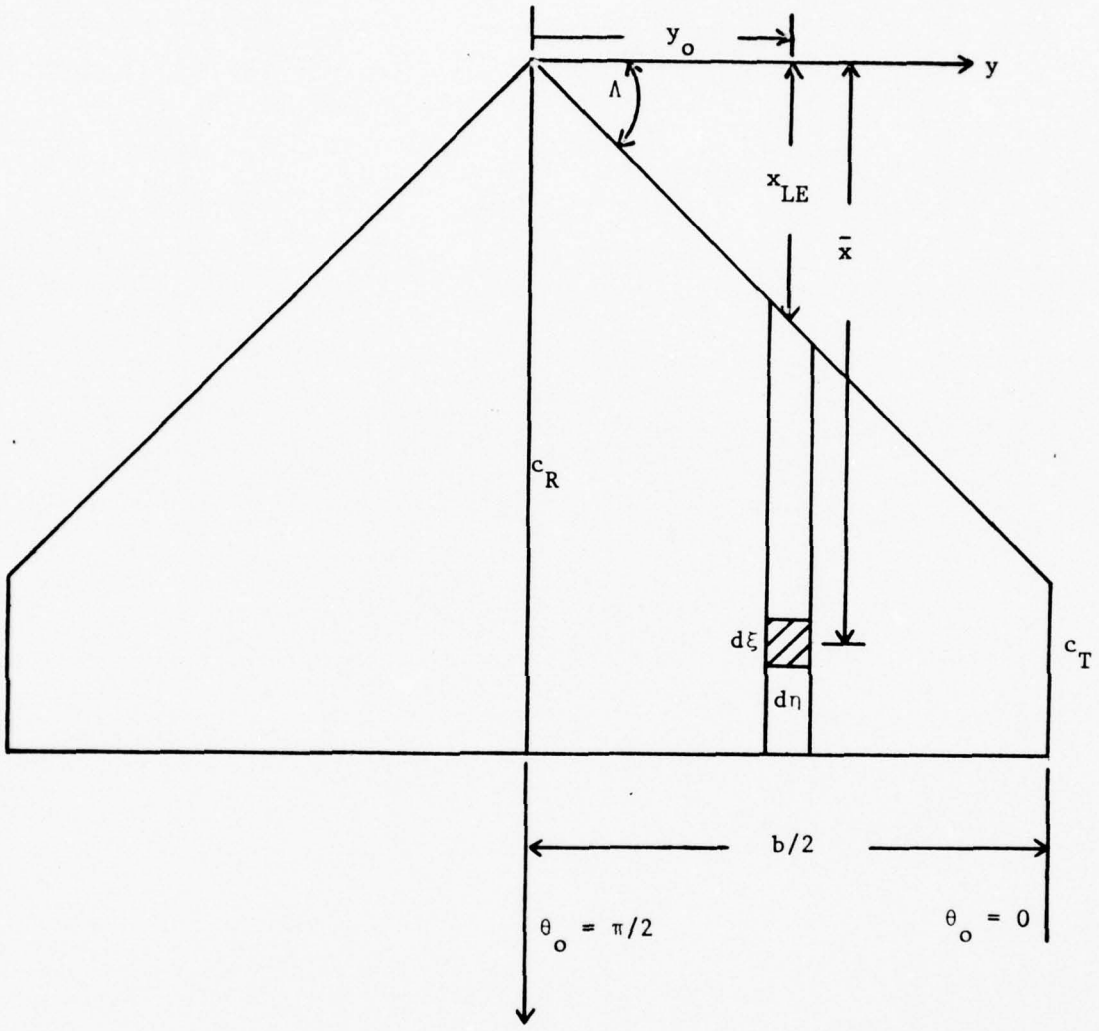


Figure 1. Schematic of the Wing Geometry and Coordinate System.

where $F_m = \sum_{n=0}^{N} B_{nm} I_{n+1}$ and $G_m = \int_0^{\pi/2} \sin 2\theta_o \sin (2m+1)\theta_o \, d\theta$.

Note that the first term in Equation (26) is the moment contribution due to wing taper, and the third term is the contribution due to leading edge sweep. The second term looks very much like the classical Glauert term from lifting line theory.

The preceeding equations constitute a set which determines the fundamental parameters of interest; lift, induced drag, and pitching moment for a thin wing in subsonic compressible flow. Before proceeding with extensions of the analysis to elevons, comments on the accuracy of the theory are in order.

The success or failure of any theory rests on its agreement with experiment; however, before comparing with experiment the accuracy of the flowfield model should first be determined. The tangency of the flow to the wing surface indicates both how well the ΔC_p distribution has been represented and to what degree the wing has been replaced with a solid surface. Obviously, low aspect ratio delta wings are the severest test for planar lifting surface theories due to the decreasing area and large ΔC_p gradients near the wing tips. Figure 2 shows the distribution of α-w, or net normalwash, over the surface of a delta wing of aspect ratio 2. From the present analysis, less than two percent deviation (0.02α) from the desired zero value is obtained except near the leading edge, which indicates that most of the wing has indeed been replaced by a solid surface. The behavior near the leading edge is due to computer difficulties in

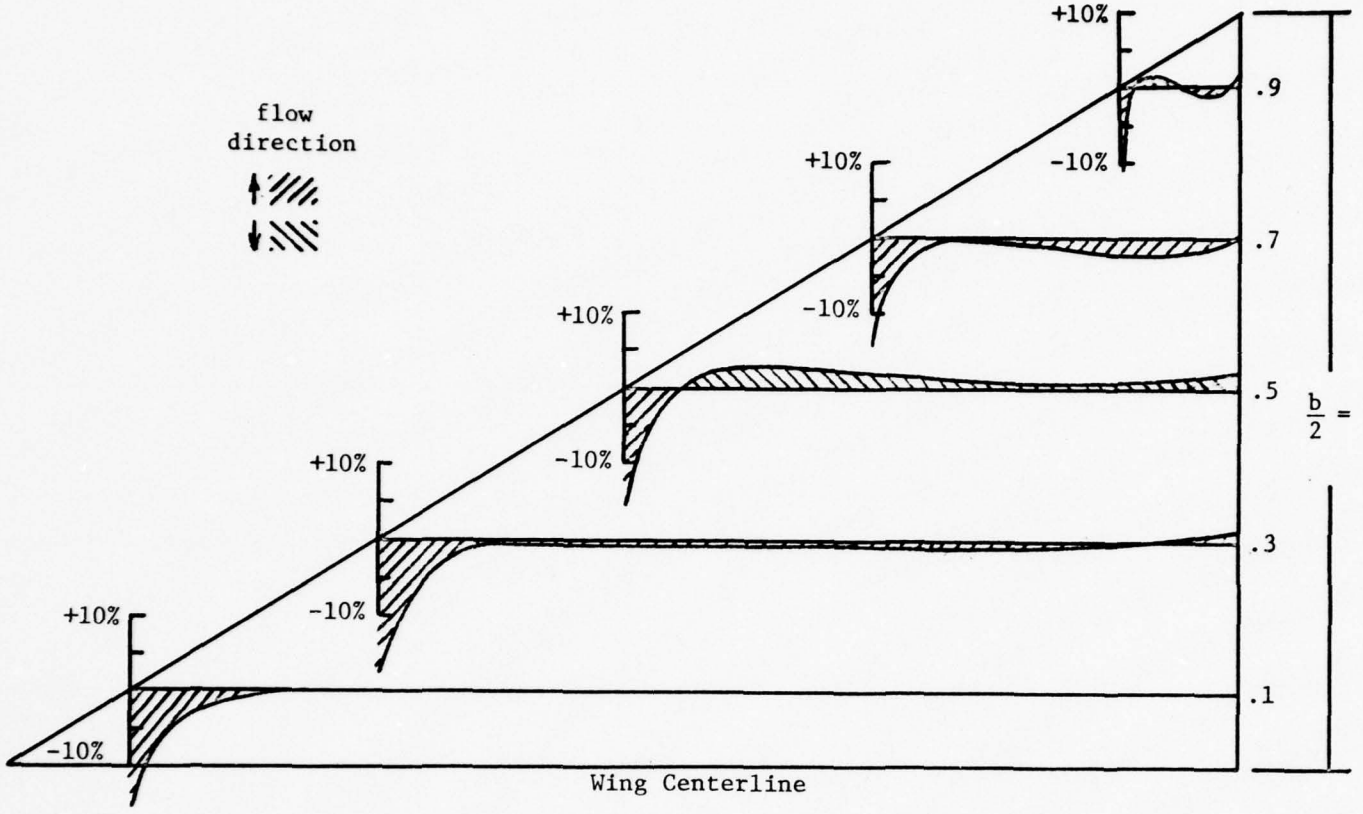


Figure 2. Downwash Distribution.

evaluating $\sqrt{(1-\xi)/\xi}$ near $\xi=0$. Compared to the flowfields in vortex lattice theory, even the errors near the leading edge and the tips would be considered minor.

ΔC_p Distribution

In addition to the net normalwash distribution shown in Figure 2, a comparison was made with experimental data for the pressure distribution over the delta wing (Wick wing) sketched in Figure 3. Results of one of these comparisons is shown in Figure 4. The experimental data extracted from Ref. (38) agrees very well with the theory except for the differences near the leading edge. These deviations are easily accounted for due to the wing thickness.

Lift and Pitching Moment Results

To illustrate the utility and accuracy of the lift and pitching moment calculations of the analysis, several wing geometries were evaluated. In Figure 5, two wings with the same leading edge sweep angle, 40°, but different taper ratios were evaluated. The spanwise lift distribution agrees very well with experimental data and the spanwise center of pressure and hence the section pitching moment is essentially within experimental error.

The measured and predicted C_{L_α}'s for low aspect ratio delta wings are shown in Figure 6. The theoretical curves properly approach the slender wing theory results for very small aspect ratios, and tend toward 2π as $AR \to \infty$.

Figure 7 shows the effect of Mach number on the theoretical and experimental lift curve slopes of two thin wings. The agreement between

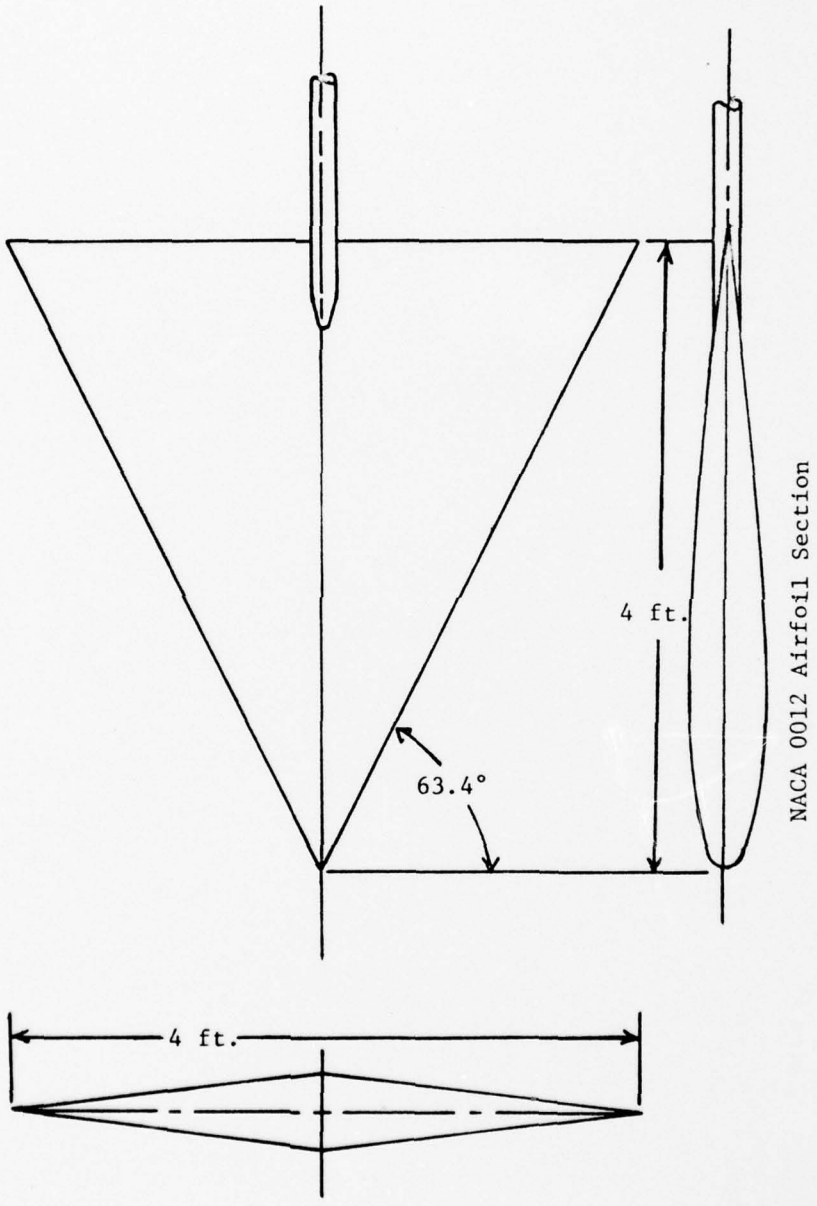


Figure 3. Sketch of Thick Wing Model (Reference 38).

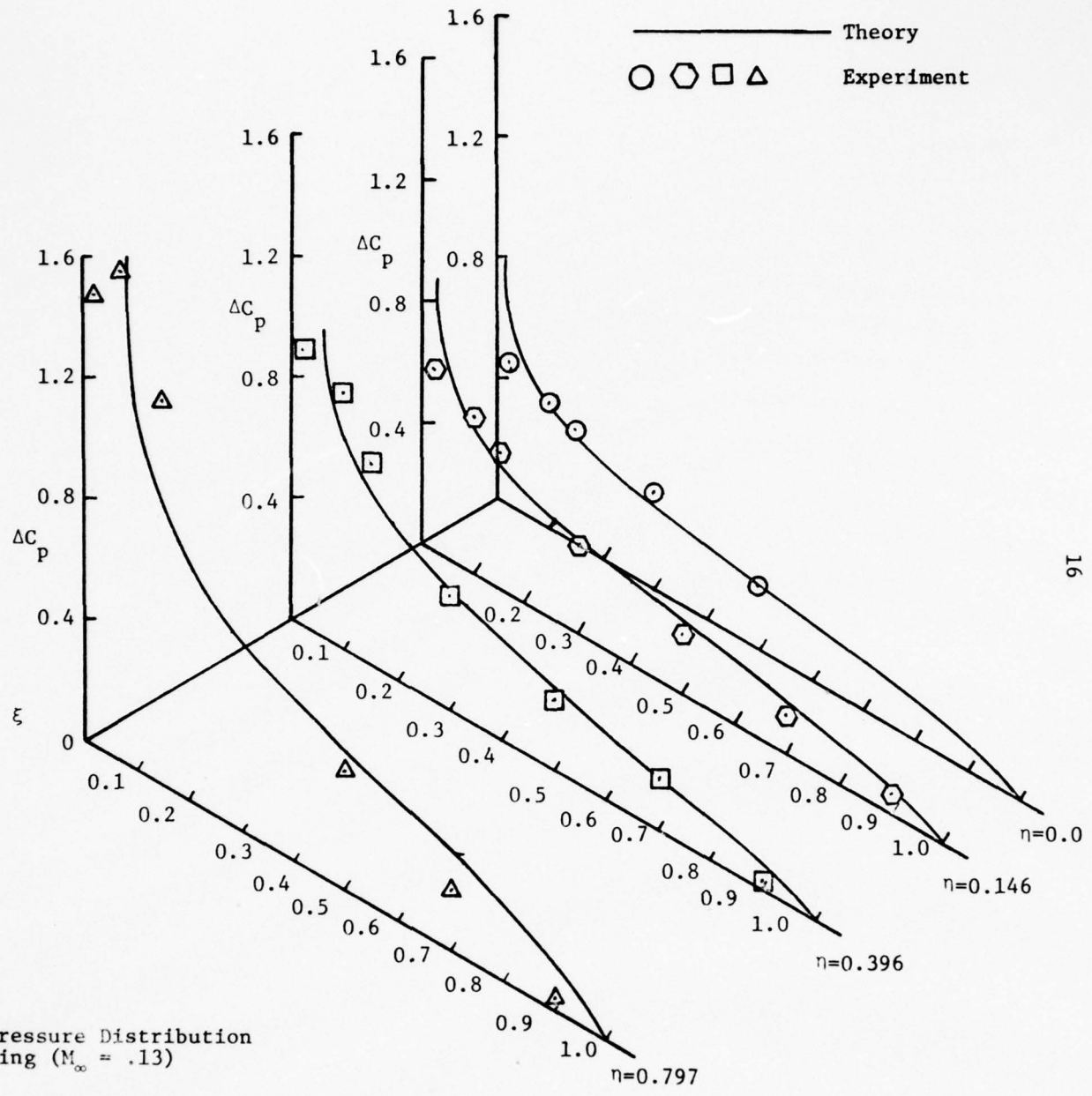


Figure 4. Planform Pressure Distribution on Delta Wing (M_∞ = .13)

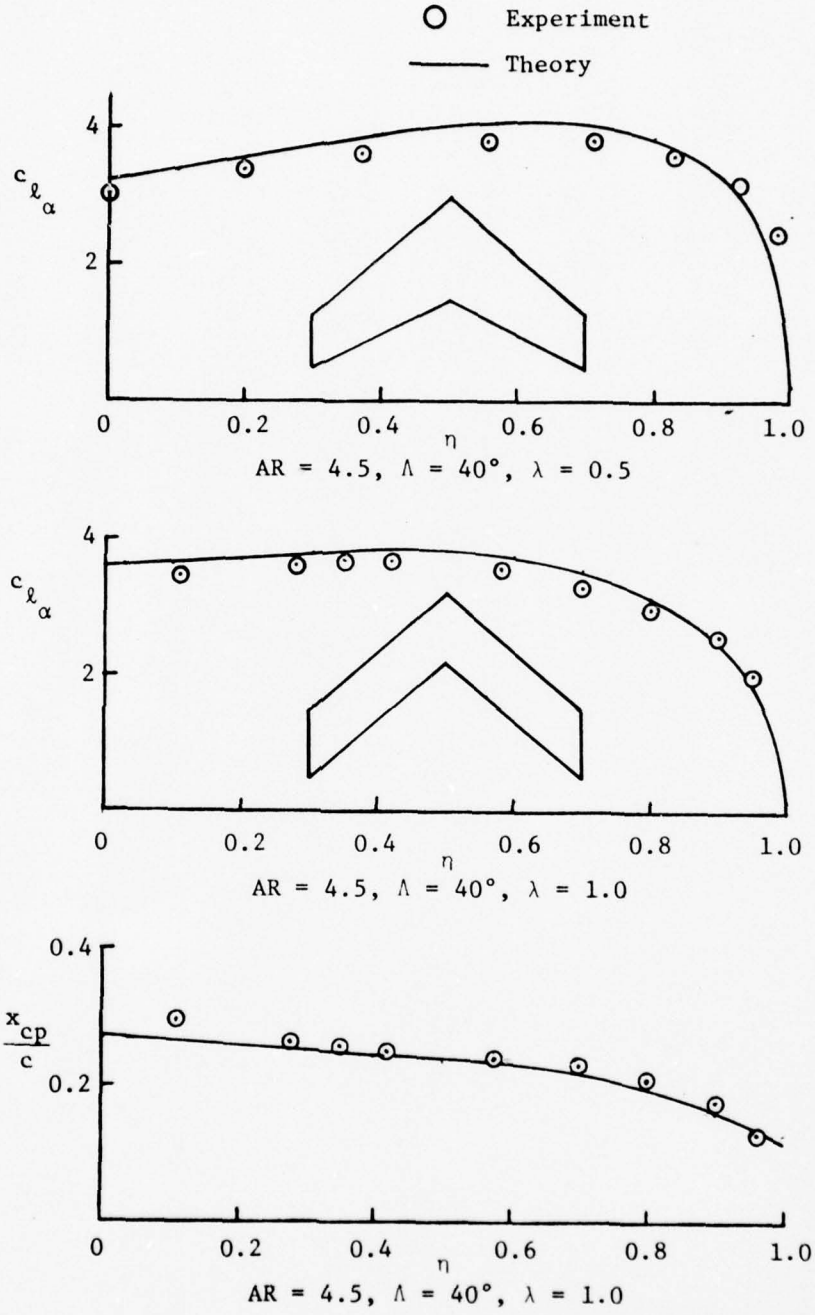
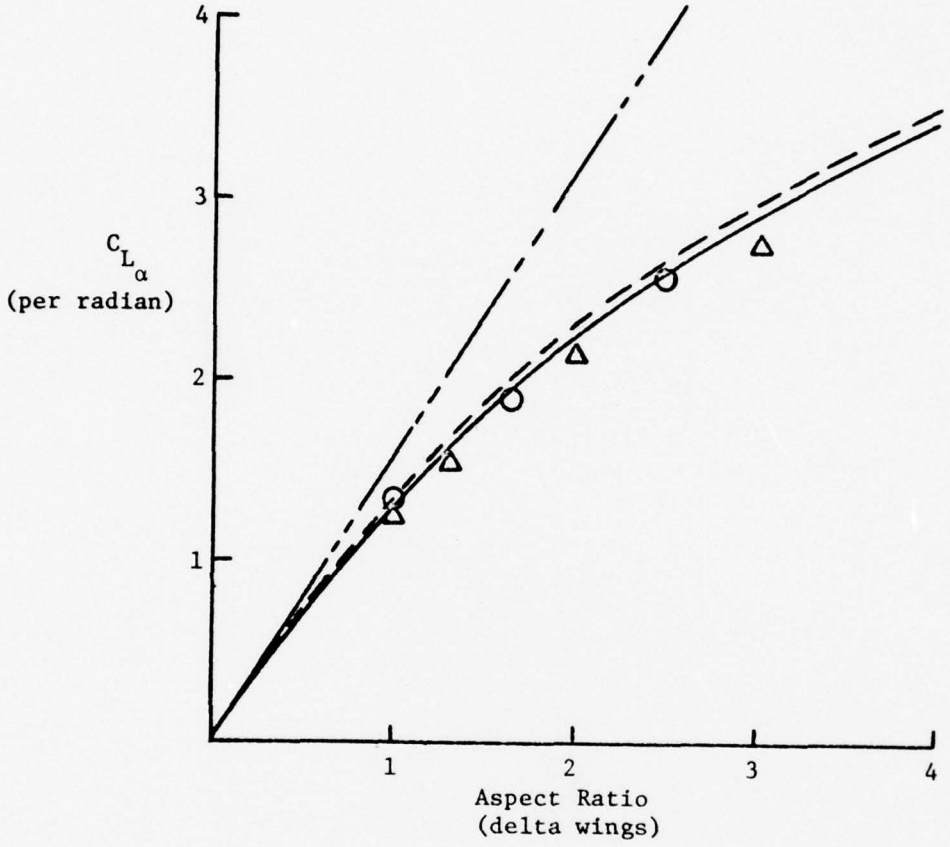


Figure 5. Spanwise Loading and Center of Pressure.



Experiment △ ○

Theory
—— Present Method
- - - Numerical Integration
—·- Slender Wing

Figure 6. Lift Curve Slopes for Delta Wings.

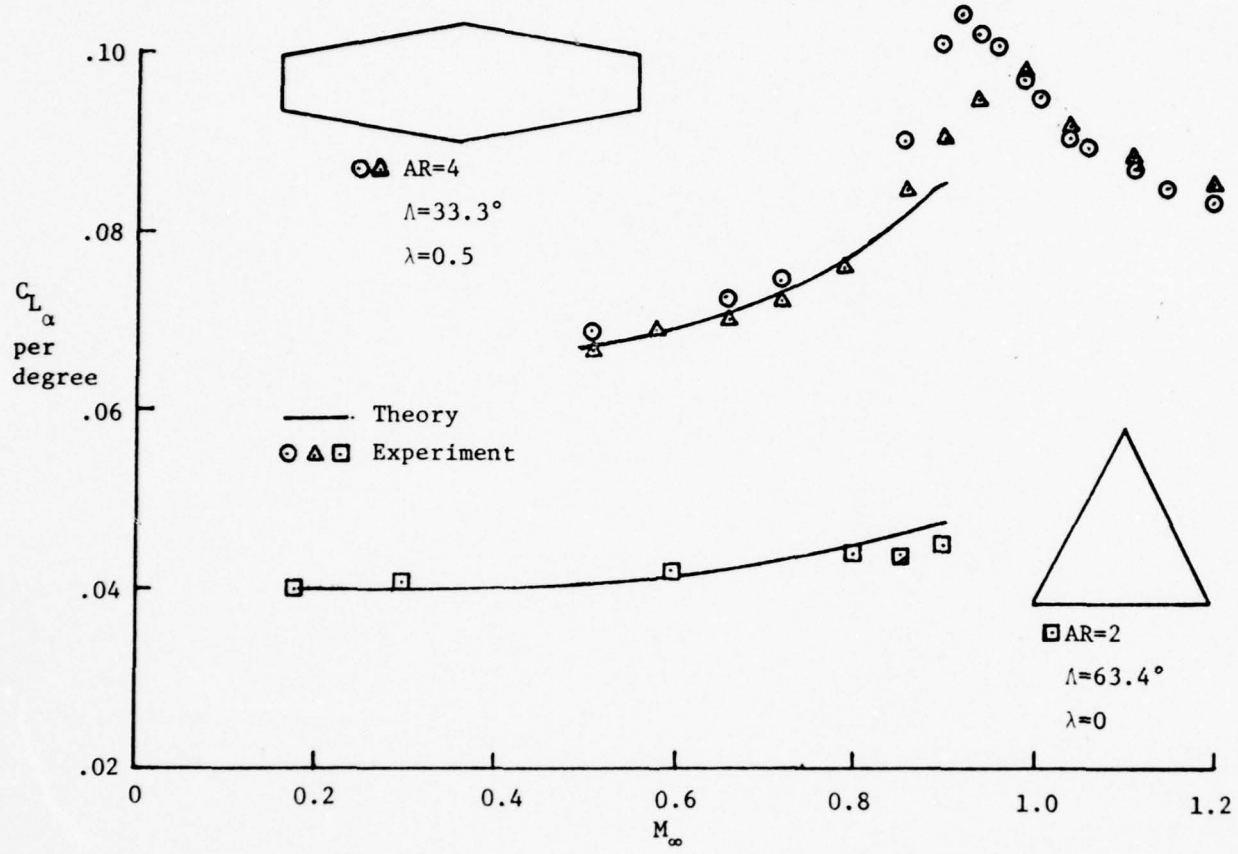


Figure 7. Mach Number Effect on Lift Curve Slopes.

theory and experiment is excellent for Mach numbers less than approximately 0.85. The good agreement above M = 0.6 is due to several factors: (1) both wings are ideally suited to a planar wing analysis since the thickness-to-chord ratios of both wing sections are less than five percent; (2) the experimental C_{L_α}'s were evaluated at low angles of attack; (3) and, most significantly, the compressibility factor β enters the theoretical equations in the same manner as in slender body theory (Ref. 3); therefore, based on slender body theory results, the true transonic region should be much smaller than that usually assumed in wing theory.

Thickness Effects

Although thickness is not considered to be a major analytical objective in the present analysis, thickness effects were considered. As an example, the wing sketched in Figure 3 is relatively thick at least along the centerline. Section lift coefficients for this wing at various angles of attack are presented in Figure 8. In this figure, no corrections have been made for thickness and still the agreement between theory and experiment is relatively good. The corresponding center of pressure (and hence pitching moment) calculation is shown in Figure 9 with excellent agreement with experimental data.

To account for thickness, two approaches were considered. First, the existing lifting surface program was modified so that boundary conditions were met on the wing surface as opposed to the "thin wing" planar surface. Results of this analysis is shown in Figure 10.

In the second approach, the wing subpanels were overlaid with source panels. This approach proved to be rather lengthy and complex but results

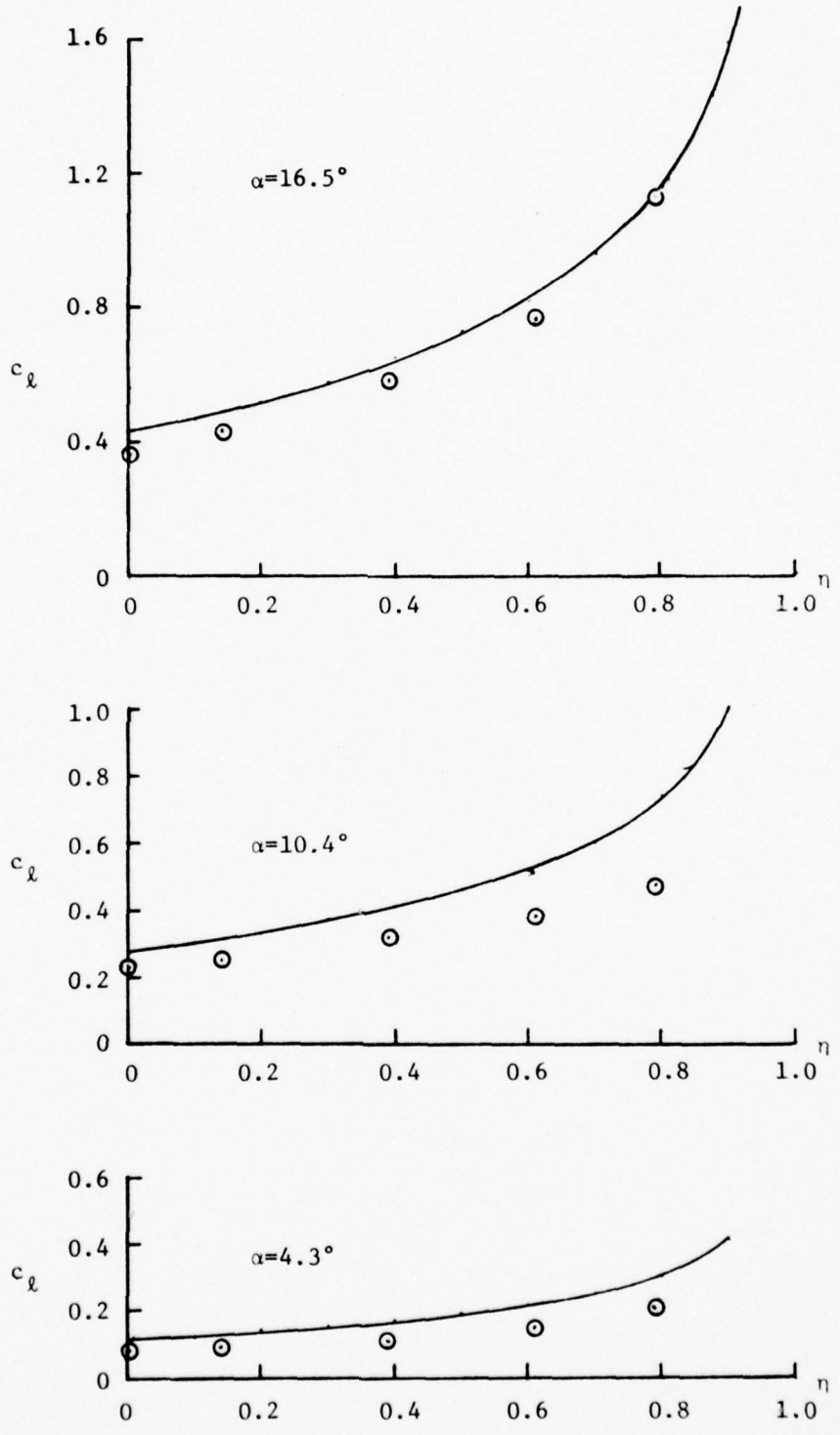


Figure 8. Spanwise Variation of Sectional Lift Coefficient at Various Angles of Attack.

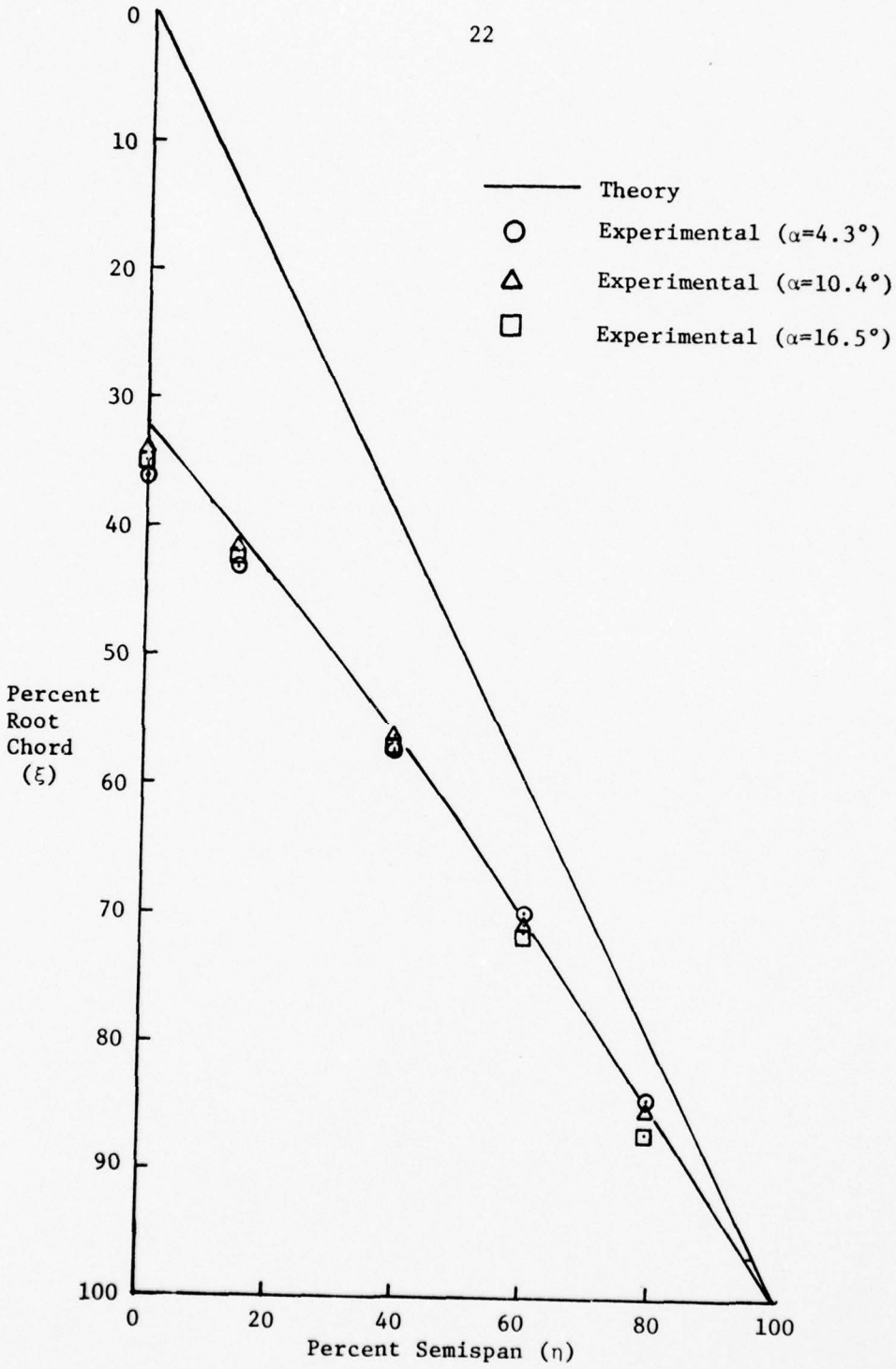


Figure 9. Center of Pressure on Wing Planform.

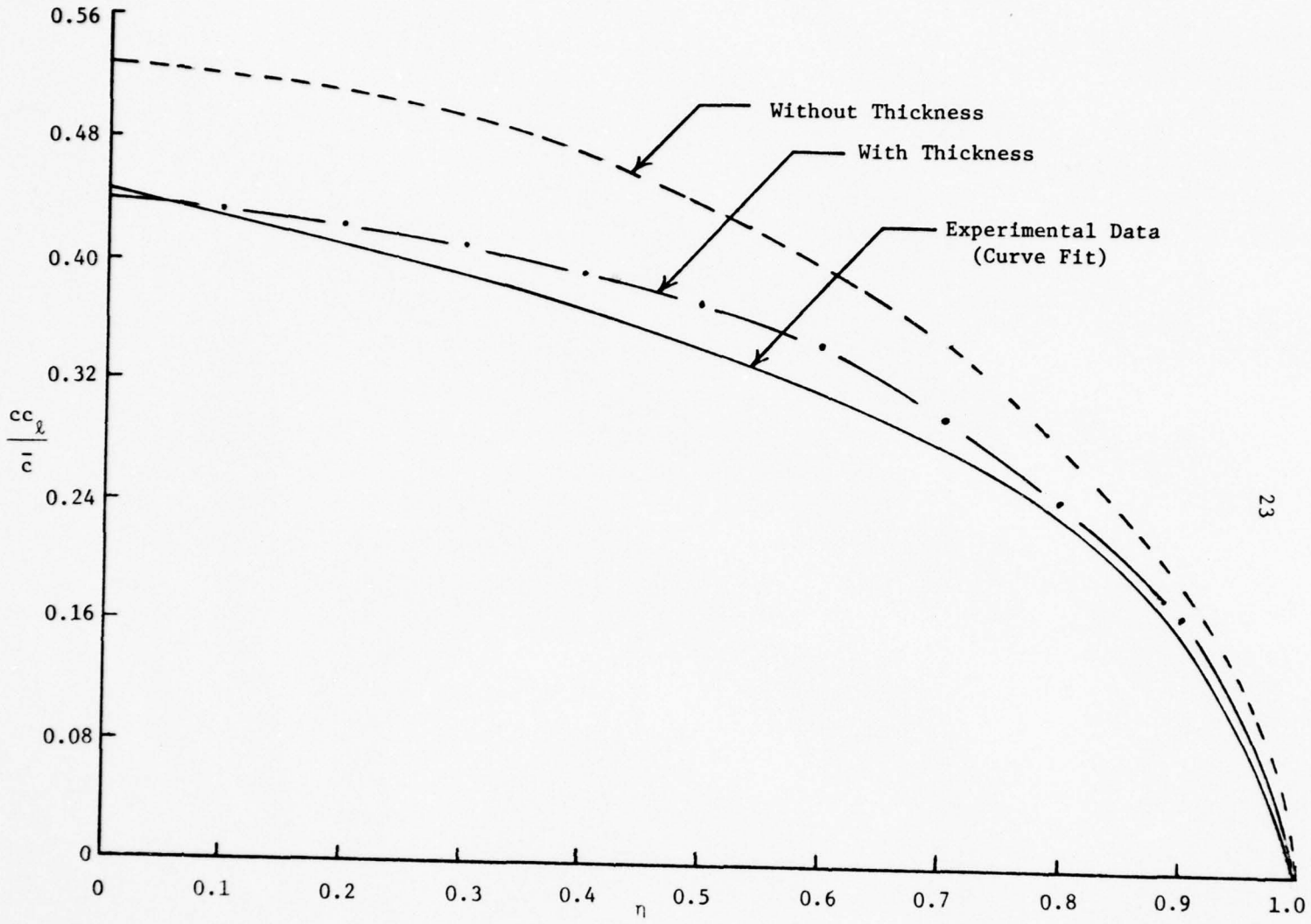


Figure 10. Spanwise Loading for Thick Wing (Wick).

were obtained which indicated that this was indeed a feasible approach. However, because of its long computer run time and large storage, the procedure was not included in the main analysis and computer program.

Elevon Loading and Hinge Moments

When a control surface (elevon) is added to a wing at the trailing edge, obviously the loading distributions on the wing will change. For a deflected elevon, a discontinuity exists in the wing surface slope and theoretically the velocity and hence the pressure differential is infinite at the hinge line. For the present anlaysis it is assumed that the hinge line for the elevon is at the elevon leading edge or wing trailing edge. Additionally, it is assumed that the elevon span is that of the wing and that the hinge line is perpendicular to the wing centerline (root chord). The analysis under these assumptions parallels that of the basic wing with the exception of the loading functions.

Two approaches were considered in the analysis of the wing loading with a deflected elevon. Glauert (39) used a single function Fourier series to represent the two-dimensional chordwise load distribution. However, a very large number of terms are required in order to adequately represent the discontinuity at the elevon leading edge. Since the techniques used in this analysis is somewhat "self-correcting" a simpler single function was initially used to represent the wing loading as

$$\Delta C_p = F(\eta)\xi^n\left[\sqrt{\frac{1-\xi}{\xi}} + c \sin \delta\sqrt{\frac{1-\xi}{|\xi-\xi_H|}}\right] \qquad (27)$$

Results using a function of this type, Equation (27), proved to be very successful in predicting the ΔC_p distribution; however, integration of the pressure distribution over the wing is rather difficult and must be done numerically. Schematically, the loading for the wing using Equation (27) is shown in Figure 11a. Because of the difficulty in integration (no closed formed solution) the single function approach was temporarily shelved and a second method was tried.

In the second approach, two functions were used; one to represent the wing loading and one to represent the elevon loading. For the wing loading term, the leading edge singularity is modeled as before but the Kutta condition is not satisfied at the trailing edge of the wing. The elevon loading term has the required leading edge singularity and the Kutta condition is satisfied at the trailing edge of the elevon. The loading function for the two functions' approach is shown in Figure 11b.

The vorticity (or ΔC_p) at any point on the wing or elevon is determined by solving the set of equations as defined by Equation (12); however, loading of the matrix is somewhat more complex. For points on the wing, the boundary condition is (as before for the wing above) sin α. However, on the elevon, the boundary condition is sin $(\alpha+\delta)$ where δ is the elevon deflection angle relative to the wing.

In order to clearly illustrate the method by which the unknown coefficients, B_{nm}, are determined, consider an example wing as shown in Figure 12a. Suppose 4 control point locations are placed on the wing in the chordwise direction, 4 on the elevon in the spanwise direction and 2 on the elevon in the chordwise direction. Schematically, the control points would appear as shown in Figure 12a.

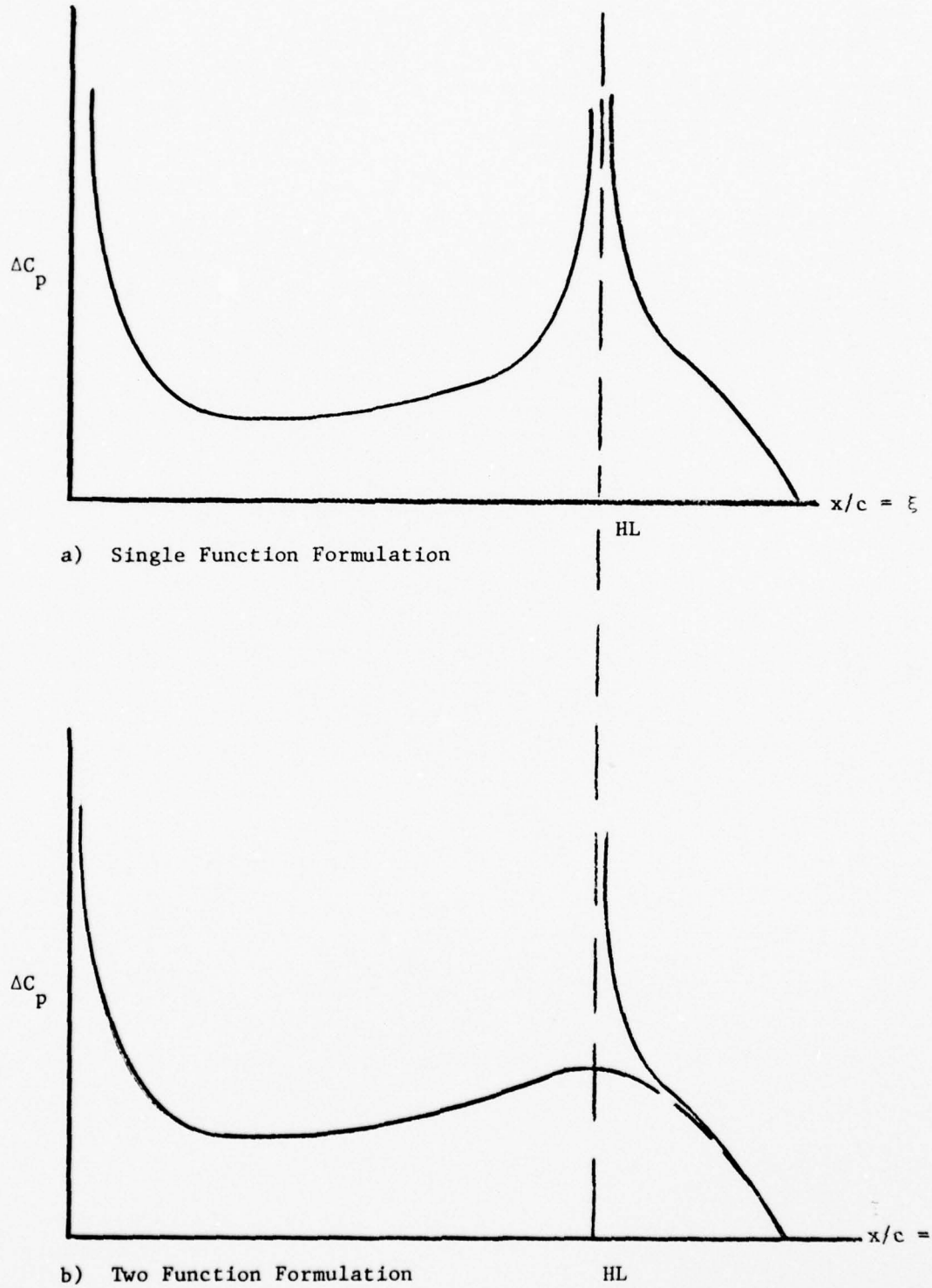
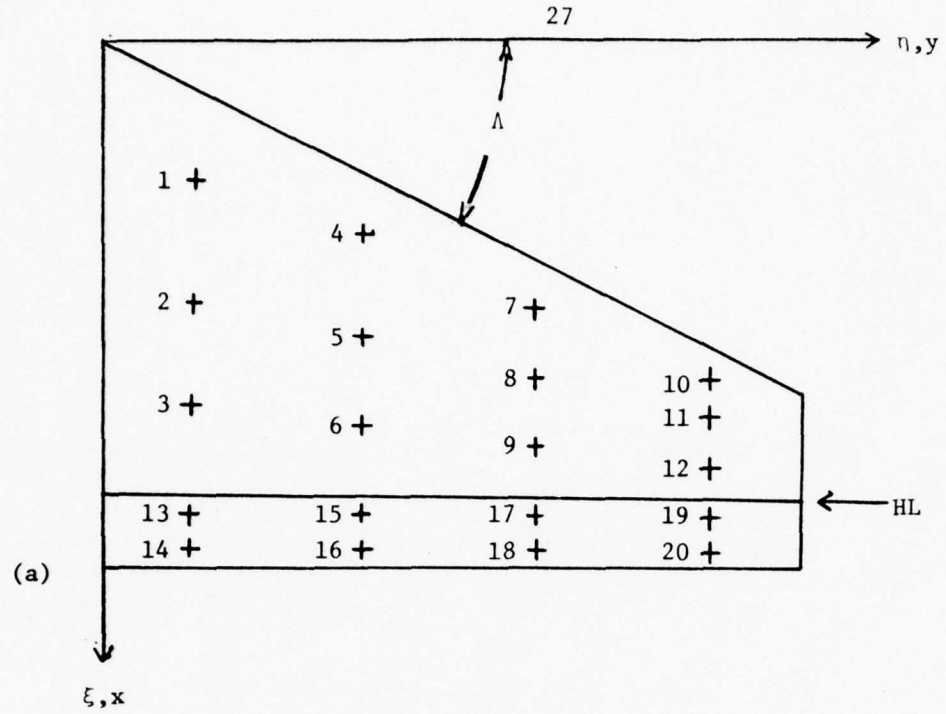
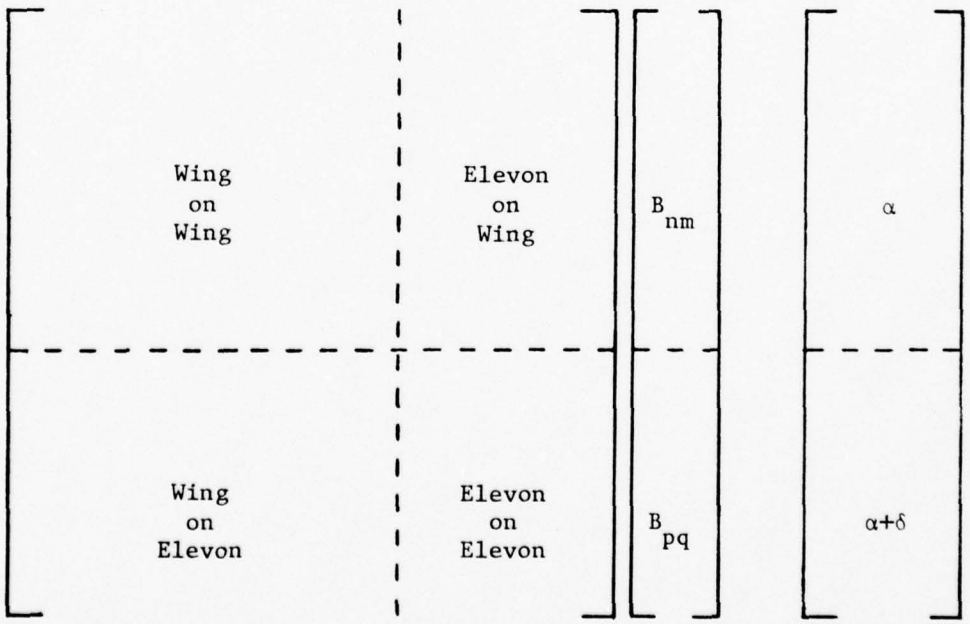


Figure 11. Typical Chordwise Loading Functions.



(a)



(b)

Figure 12. Typical Control Point Locations and Matrix Schematic for Wing-Elevon Configuration.

The matrix for determining the unknown B's is shown in Figure 12b. Note that any one row of the coefficient matrix represents the velocities induced at one control point. The numbering scheme for the control point locations is also shown in Figure 12. The B_{nm}'s are the coefficients associated with the wing loading function and the B_{pq}'s are associated with the loading function for the elevon. Once the B's have been determined, the loading on the wing or elevon may be computed independently as shown in the next section.

Sectional Loads and Moments

The sectional lift for a wing with a deflected elevon is

$$cc_{\ell}(y_o) = \int_{x=0}^{x=x_H} \Delta C_{p_w}(\xi,\eta)\, d_x + \int_{x=x_H}^{x=c_T} \Delta C_{p_E}(\xi,\eta)\, dx \tag{28}$$

where the total chord length is

$$c_{To} = c_W + c_E \tag{29}$$

As before (for the wing alone) define

$$\xi = x/c_{To} \tag{30}$$

Then the first integral for the wing becomes

$$cc_{\ell_w} = c_{To} \int_{\xi=0}^{\xi=\xi_H} \Delta C_{p_w}(\xi,\eta)\, dx \tag{31}$$

For the second integral define

$$\xi_E = (x-x_H)/c_E \tag{32}$$

and Equation (28) may then be written as

$$cc_{\ell} = c_{T_o} \int_{\xi=0}^{\xi=\xi_H} \Delta C_{p_w} \, d\xi + c_E \int_{\xi_E=0}^{\xi_E=1} \Delta C_{p_E}(\xi_E, \eta) d\xi_E \tag{33}$$

Now, for the wing

$$\Delta C_{p_w} = \sum_{n=0}^{Nw} \frac{1}{c(\eta)} \sum_{m=0}^{M} B_{nm} \sin(2m+1)\theta \; \xi^n \sqrt{\frac{1-\xi}{\xi}} \tag{34}$$

In order to evaluate the first integral in Equation 33, define

$$I_{wn} = \int_0^{\xi_H} \xi^n \sqrt{\frac{1-\xi}{\xi}} \, d\xi, \quad n=0,1,2\ldots,N_w \tag{35}$$

Integration of Equation (35) yields

$$I_{wo} = \pi/4 + \sqrt{\xi_H - \xi_H^2} + \frac{1}{2} \sin^{-1}(2\xi_H - 1) \tag{36}$$

where

$$\xi = x/c_{T_o} = x/(c_w + c_E)$$

or

$$\xi_H = c_w(\eta)/(c_w(\eta) + c_E)$$

For other values of n, Equation (35) becomes

$$I_{wn} = \frac{1}{n+1} \left[\frac{2n-1}{2} I_{n-1} - \xi_H^{n-2} (\xi_H - \xi_H^2)^{1.5}\right] \tag{37}$$

For the second integral in Equation (33), the results are for the elevon

$$I_o = \pi/2 \tag{38}$$

and

$$I_p = \frac{2p-2}{2p+2} I_{p-1} \tag{39}$$

Hence,

$$cc_\ell = c_{T_o}\left[\sum_{n=0}^{N_w} \frac{1}{c(\eta)} \sum_{m=0}^{M_w} I_{wn} B_{nm} \sin(2m+1)\theta\right]$$

$$+ c_E \left[\sum_{p=0}^{N_E} \frac{1}{c_E} \sum_{q=0}^{M_E} I_{pq} B_{pq} \sin(2q+1)\theta\right] \tag{40}$$

The total lift for the wing then becomes

$$C_L = \frac{1}{s}\int_{-b/2}^{b/2} cc_\ell(\eta)\, d\eta = \frac{2}{S}\int_0^1 cc_\ell\, d\eta \tag{41}$$

Evaluation of Equation (41) is not easily done analytically and hence the integral is done numerically using the trapezoidal rule. The reason for the difficulty lies in the fact that for a general wing planform shape, ξ_H is a function of η and hence even for n=0 the integral is very complex. For the elevon alone, one could in fact find the closed form solution for the total lift (on the elevon).

The pitching moment for the entire wing and elevon is found by evaluating

$$C_m = \frac{2}{S\bar{c}}\int_0^1 cc_{mrc}\, d\eta \tag{42}$$

where cc_{mrc} is the section pitching moment about the y axis as shown in Figure 1. Equation (42) is also evaluated numerically.

Of particular interest where the elevon is concerned is the computation of the elevon hinge moment. This could be extracted numerically from Equation (42); however, it may be computed in closed form. The moment coefficient about the hinge line is (See Fig. 13)

$$C_H = -\frac{1}{S\bar{c}_E}\int_{-b/2}^{b/2} cc_{\ell_E}(y)\,\bar{x}_E(y)dy \tag{43}$$

or

$$C_H = \frac{2}{S\bar{c}_E}\int_0^1 cc_{\ell_E}(\eta)x_{cp_E}\,d\eta = -\frac{2}{S\bar{c}}\int_0^1 cc_{mE}\,d\eta \tag{44}$$

where

$$cc_{mE} = c_E{}^2\int_0^1 \Delta C_{p_E}\,\xi d\xi \tag{45}$$

and

$$\xi = (x-x_H)/c$$

The ΔC_p distribution for the elevon is (see Equation (34) for the wing).

$$\Delta C_{p_E} = \sum_{p=0}^{N_E}\frac{1}{c_E(\eta)}\sum_{q=0}^{M_E} B_{pq}\sin(2q+1)\theta\,\xi^p\sqrt{\frac{1-\xi}{\xi}} \tag{46}$$

Following the general procedure as outlined for the wing, the elevon hinge moment is evaluated by substituting Equation (46) into Equation (44) and the result is

$$cc_{mE} = c_E\sum_{q=0}^{M_E}\sin(2q+1)\theta[E_q] \tag{47}$$

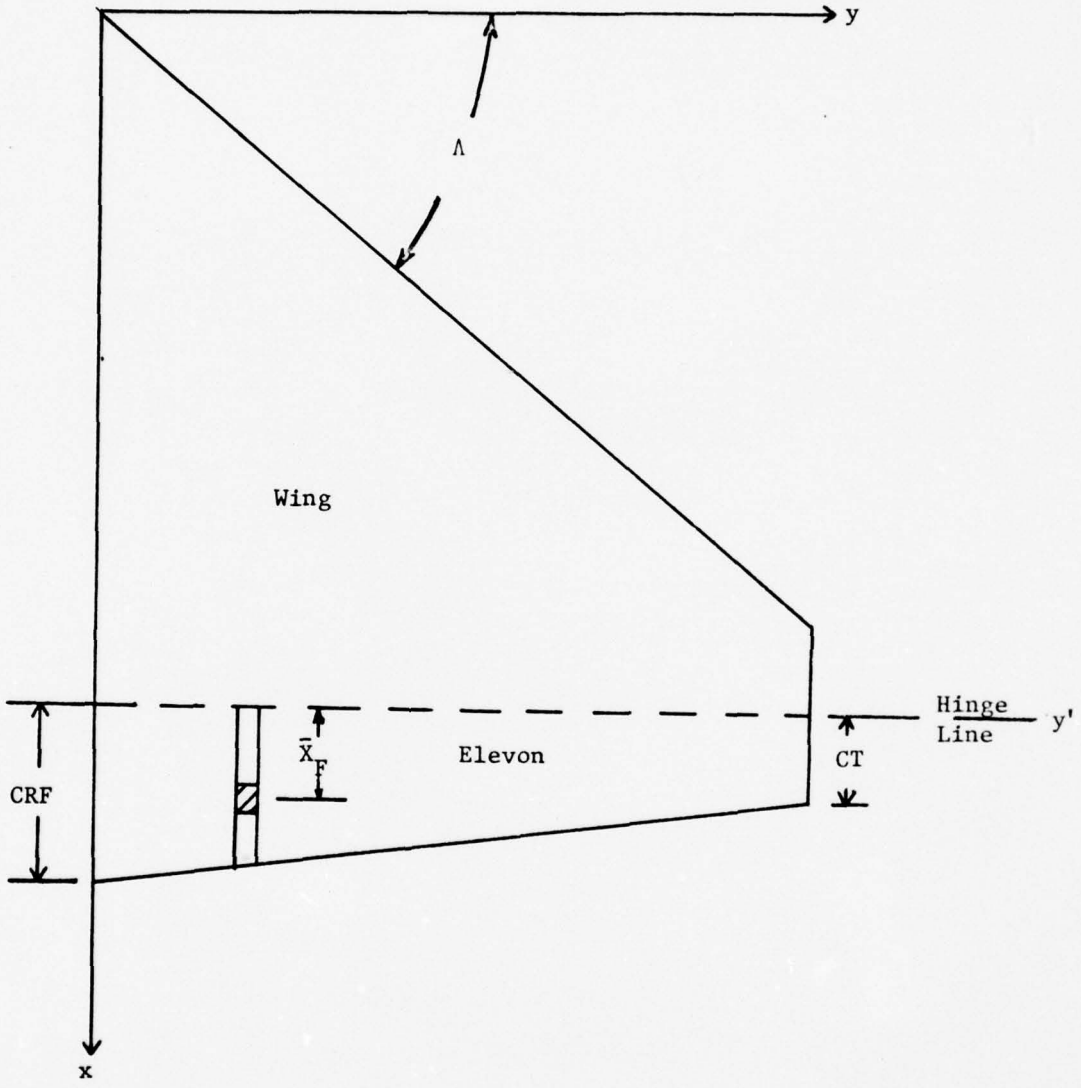


Figure 13. Schematic for Coordinate System for the Elevon.

where

$$F_q = \sum_{p=0}^{N_E} B_{pq} \, I_{p+1} \tag{48}$$

and

$$I_{p+1} = \int_0^1 \xi^{p+1} \sqrt{\frac{1-\xi}{\xi}} \, d\xi \tag{49}$$

Finally, Equation (47) is substituted into Equation (44) and the result is

$$C_H = - \frac{2c_{RE}}{S\bar{c}_E} \left[\frac{\pi}{4} F_1\right] + \frac{c_{RE}-c_{TE}}{S\bar{c}_E} \sum_{q=0}^{M_E} F_q \, G_q \tag{50}$$

where $G_q = \int_0^{\pi/2} \sin 2\theta \sin [(2q+1)\theta] d\theta$

Results of Elevon Loading Computations

At the present time the elevon-wing analysis and results are in the beginning stages and very little experimental data seems to be available for comparison purposes. However, "some" experimental data was found for four wings ranging in aspect ratios from 2 to 6 and results are shown in Figure 14.

In Figure 14, experimental values of C_{L_α} and C_{L_δ} are compared with the present theory with satisfactory results. The theory utilizes the two-function approach and is within experimental error of the data.

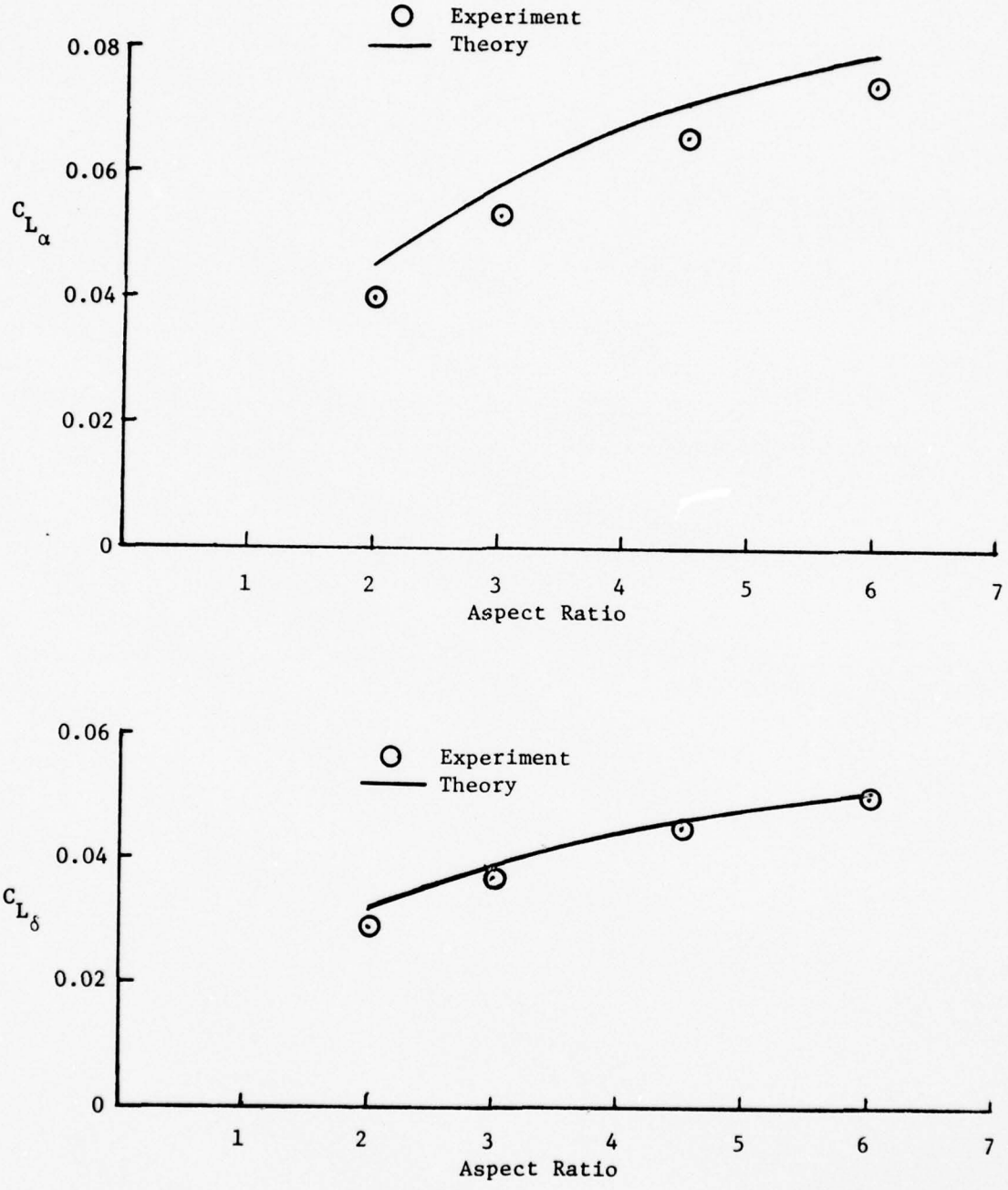


Figure 14. Aerodynamic Coefficient C_{L_α} and C_{L_δ} versus Aspect Ratio.

In summary, the objectives for the research effort for the first year have been accomplished. Excellent results have been obtained in some areas and areas where further concentrated efforts are required have been identified.

SUPERSONIC ANALYSIS

Current Methods

There are several methods available for solving supersonic potential flow problems. These include exact theories, discrete element methods, kernel function methods, and numerical approached (finite element or finite difference) schemes. All potential flow methods may be grouped in one of two categories: linear theory or full potential (nonlinear numerical approach).

Numerical methods for solving the nonlinear potential equations, such as finite difference techniques, provide the most accurate solutions available. These methods were not considered for the current problem, however, due to the high cost and excessive computation times usually required.

Linearized theory methods, based on the superposition of elemental solutions of the linearized differential equation governing the flow, have been employed extensively in analysis of supersonic aircraft. Exact theories, discrete element methods and kernel function methods are all in the realm of linear theory.

Several exact linear theory methods are available, such as Slender Body Theory (44), Conical Flow Theory (43) and Evvard's method (28,45). Slender Body Theory uses two-dimensional crossflow and slender wing-body ideas to generate general forces and moments for an entire configuration.

Details of the pressure loading are not available and general deformed wings cannot be handled. Conical flow theory gives exact equations for ΔC_p over thin flat wings with subsonic leading edges at constant angle of attack. Evvard's theory involves source sheet integrals representing wings with supersonic leading and trailing edges. Exact expressions for ΔC_p based on Evvard's theory have been derived for constant angle of attack, constant roll rate, and constant pitch rate. The general formulation is also the basis for several discrete element methods. Unfortunately, none of these methods give results which are generally applicable to a deformed wing study. The solutions do, however, give insight into flow patterns and load distribution trends, and can be used as limiting check cases for a deformed wing method.

Discrete element methods are computerized numerical techniques which use elemental source and vortex solutions, in conjunction with the superposition principle, to model the flow over general configurations. In these methods the wing is subdivided into a mesh or grid, each panel of which is a source or vortex sheet of constant, but usually unknown, strength. The unknowns are found either by inverting a large influence coefficient matrix, representing the flow tangency condition at selected points of the wing, or by a downstream marching technique. Current methods are available which can solve problems with thousands of panels; however, the cost per solution increases with increasing number of panels. Examples of the discrete element method include the approaches of Etkin (46) and Purvis (47), which are based on Evvard's Theory, the well known Woodward technique (7), which uses source and vortex elements, the "Mach box" method of Pines and Dugundji (48), and the panel method of Appa and Smith (49).

Supersonic kernel function methods have also been developed with varying degrees of success. Some analysts, such as Cunningham (32) and Curtis and Lingard (50), use assumed functions to solve the wing problem in the same manner as that employed in subsonic kernel function methods. Others, such as Miranda (51) and Carlson, et al, (52,31,53), solve the kernel integral in a manner similar to the discrete element approaches. The most serious disadvantage of the kernel function method is that planforms with discontinuous pressure distributions are very difficult to treat. Since the assumed pressure functions are smooth, the convergence to a discontinuous distribution is very slow. When discrete elements are used, high frequency disturbances propagate along Mach lines and may increase in amplitude. Cunningham (32) avoided the former problem by using exact theory weighting functions, which contain the appropriate discontinuities. In the latter case, Carlson, et al (31,53,28), employed a "terminal smoothing" procedure to eliminate the undesired wiggles.

The present method proposes to combine the assumed pressure function approach for solving the supersonic kernel integral with the discrete element technique. Results will show that this approach retains the speed and accuracy advantages of the kernel function method without encountering any of the previously mentioned problems.

Theoretical Approach

A thin planar lifting surface in supersonic flow may be represented mathematically by a finite sheet of elemental horseshoe vortices in the same manner as in subsonic flow (Ref. 21). The nondimensional velocity potential for such a surface is (See Appendix)

$$\phi(x,y,z) = \frac{1}{2\pi} \iint_{S_o} \frac{\gamma(x_o,y_o)}{(y-y_o)^2+z^2} \; z\left[\frac{(x-x_o)}{\sqrt{(x-x_o)^2-\beta^2(y-y_o)^2-\beta^2z^2}}\right] dx_o dy_o \qquad (51)$$

The variables of integration x_o, y_o are defined only over the planform surface, S, and $\gamma(x_o,y_o)$ is the unknown vorticity. Equation (51) differs from the subsonic result by (1) the term in brackets, (2) the factor 2π instead of 4π, and (3) the region of integration S_o includes only that portion of the wing surface S which is contained in the Mach forecone from point (x,y,z).

The relation between the pressure loading coefficient ΔC_p and the vorticity is the same as that for subsonic flow. Applying the Kutta-Joukowski Theorem at a point on the sheet gives

$$\gamma(x_o,y_o) = \frac{\Delta C_p(x_o,y_o)}{2} \qquad (52)$$

where $\Delta C_p = C_{p_{lower}} - C_{p_{upper}}$.

The nondimensional perturbation velocity w, or downwash, which the lifting surface induces normal to itself is found by differentiating Equation (51) with respect to z and taking the limit as z approaches zero. This process results in

$$w(x,y) = \frac{1}{4\pi} \iint_{S_o} \frac{\Delta C_p(x_o,y_o)}{(y-y_o)^2} \; \frac{(x-x_o)}{\sqrt{(x-x_o)^2-\beta^2(y-y_o)^2}} \; dx_o dy_o \qquad (53)$$

which is the well known supersonic kernel function integral. The downwash that a lifting surface in supersonic flow induces on itself is

unique in that the downwash point is located on the boundary of the region of integration. The integral gives the appearance of being improper due to the singularity at $y=y_o$ within the region of integration. This integrand is, as previously shown, the limiting form in the z=0 plane of a more general non-singular integrand. Consequently, the integral would be expected to yield a finite result for w just as in the subsonic case. There also appears to be an upwash singularity along Mach waves through x_o,y_o due to the square root term in the denominator. As noted in Reference 31: "...this same upwash field, with the large values of upwash near the Mach cone limits, is also largely responsible for the difficulties in representing supersonic-flow phenomena by means of finite-element techniques." This problem does not appear in the current method, which contains finite-element type terms, and in fact, the influence of a discrete panel along its Mach waves will be shown to be a finite value.

Equation (53) is the starting point adopted by most authors (31,32) for the planar wing case.

The first step in solving the integral equation is to determine the form of the unknown pressure loading ΔC_p, which unfortunately appears under the integral sign. As was done in the subsonic case (Ref. 21), exact theoretical results will be used as a weighting function and multiplied by an assumed functional distribution with unknown coefficients. The form of the weighting function is particularly important in supersonic flow since the pressure distribution has sharp breaks (discontinuities in slope) along certain Mach lines. This procedure has been used successfully by Cunningham (Ref. 32). The form of the pressure loading used herein is

$$\Delta C_p(x_o,y_o) = P(x_o,y_o) \sum_{n=0}^{N} A_n(\eta)\ \xi^n \tag{54}$$

where

$$A_n(\eta) = \sum_{m=0}^{M} B_{nm} \sin(m+1)\theta \tag{55}$$

and

$$\theta = \text{Arcos}(\eta) \tag{56}$$

The nondimensional chordwise and spanwise variables ξ,η are

$$\xi = \frac{x_o - x_{LE}(\eta)}{c(\eta)} \tag{57}$$

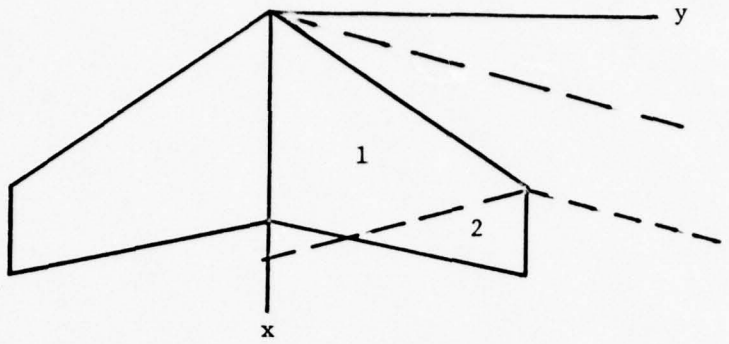
and

$$\eta = y/(b/2) \tag{58}$$

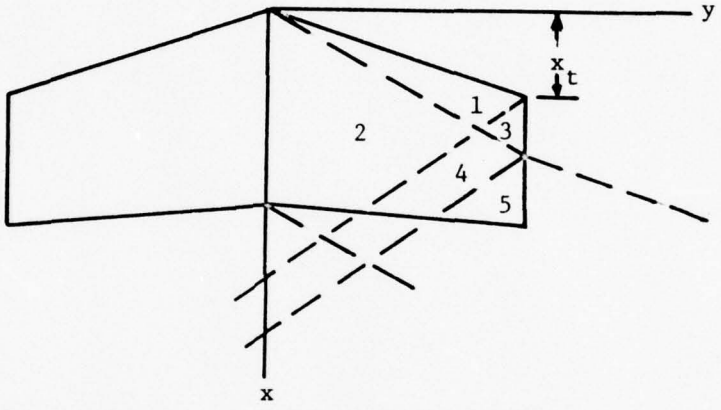
The weighting function $P(x_o,y_o)$ has several forms, depending on whether the wing leading and trailing edges are subsonic or supersonic. The forms used will be based on exact and semi-exact results for a general trapezoidal wing as shown in Figure 15.

For a subsonic leading edge and supersonic trailing edge (Fig 15a), the weighting functions used are the pressure equations given in Reference 40. These equations are based on an exact conical flow solution for region 1 and an approximation to the exact results in the tip region 2. For region 1:

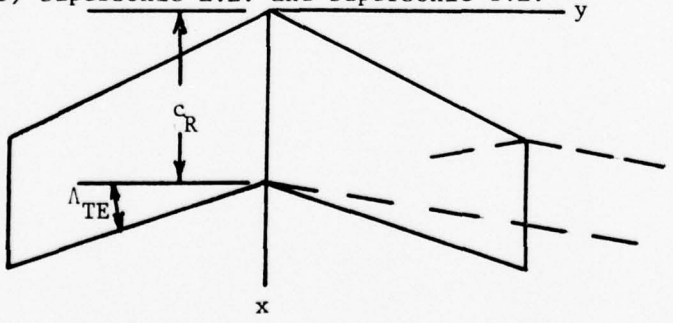
$$P(x_o,y_o) = \frac{4}{E(K)\ \sigma\sqrt{1 - \left(\frac{y_o\sigma}{x_o}\right)^2}} \tag{59}$$



(a) Subsonic L.E. and Supersonic T.E.



(b) Supersonic L.E. and Supersonic T.E.



(c) Subsonic T.E., Arbitrary Case L.E.

Figure 15. Regions of Integration for the Supersonic Kernel Function Formulation.

where E(K) is the complete elliptic integral of the second kind of modulus

$$K = \sqrt{1 - \beta^2/\sigma^2} \tag{60}$$

and $\sigma \equiv \tan \Lambda$.

In region 2, the approximate equation from Reference 40 is

$$P(x_o,y_o) = \frac{8}{\pi}\sqrt{\frac{1 - y_o}{(\beta+\sigma)(x_o+y_o\sigma)}} \tag{61}$$

When the leading edge is supersonic, there are five regions to be considered (Figure 15b). Exact equations for each region are given in Reference 41, which is based on Evvard's theory (28).

Region 1:

$$P(x_o,y_o) = P_1 = 4/\sqrt{\beta^2-\sigma^2} \tag{62}$$

Region 2:

$$P(x_o,y_o) = \frac{P_1}{\pi}\left[\text{Arcos}\left(\frac{\sigma+\beta\tau}{\beta+\sigma\tau}\right) + \text{Arcos}\left(\frac{\sigma-\beta\tau}{\beta-\sigma\tau}\right)\right] \tag{63}$$

where

$$\tau = \beta y_o/x_o \tag{64}$$

Region 3:

$$P(x_o,y_o) = P_1\left[1 - \frac{1}{\pi}\,\text{Arcos}\,\left(\frac{\tau_a\{2\beta+\sigma\}-\beta}{\beta+\sigma\tau_a}\right)\right] \tag{65}$$

where

$$\tau_a = \frac{\beta(b/2-y_o)}{x_o-x_t} \tag{66}$$

Region 4:

$$P(x_o,y_o) = \frac{P_l}{\pi}\left[\text{Arcos}\left(\frac{\sigma+\beta\tau}{\beta+\sigma\tau}\right) + \text{Arcos}\left(\frac{\sigma-\beta\tau}{\beta-\sigma\tau}\right) - \text{Arcos}\left(\frac{\tau_a\{2\beta+\sigma\}-\beta}{\beta+\sigma\tau_a}\right)\right] \quad (67)$$

Region 5:

$$P(x_o,y_o) = \frac{P_l}{\pi}\,\text{Arcos}\left(\frac{\beta+\tau_a\{\sigma-2\beta\}+2\sigma\tau_B}{\beta-\sigma\tau_a+2\sigma\tau_B}\right) \quad (68)$$

where

$$\tau_B = \frac{\beta b}{2(x_o-y_t)} \quad (69)$$

If the trailing edge is subsonic (Figure 15c), the pressure functions calculated above for either case (subsonic or supersonic L.E.) are corrected by a term which enforces the Kutta condition along the trailing edge. This term is an approximation based on the exact results for Region 3. It is used in the same manner as the one used by Cunningham (Ref 32), and is multiplied by the previously calculated pressure terms:

$$P(x_o,y_o) = P(x_E,y_o)\left[1-\frac{1}{\pi}\,\text{Arcos}\left(\frac{\tau_E\{2\beta+\sigma_{TE}\}-\beta}{\beta+\sigma_{TE}\tau_E}\right)\right] \quad (70)$$

where

$$x_E = c_R + \beta y_o \quad (71)$$

$$\tau_E = \frac{c_R+y_o\sigma_{TE}-x_o}{y_o(\sigma_{TE}-\beta)} \quad (72)$$

$$\sigma_{TE} = \tan\Lambda_{TE} \quad (73)$$

The function $P(x_E,y_o)$ is evaluated at the y_o point on the Mach line from the trailing edge vortex using the appropriate equation from (59) through (68).

With the desired form of the pressure function determined, the next task is to evaluate the integral. The following discussion will present the necessary equations. The evaluation does not proceed in the classical manner of treating kernel functions (i.e., numerical quadrature), even though functional distributions for the pressure panels from the discrete element approach (see, for example, Woodward (7)) is used to simplify the integration procedure.

First, the wing surface is subdivided into a large number of small finite elements. Equation (53) for the downwash may then be written

$$w(x,y) = \sum_{S_o} \sum \Delta w(x,y) \tag{74}$$

where $\Delta w(x,y)$ denotes the downwash at (x,y) due to an element or portion of an element in the Mach forecone from (x,y). By judiciously choosing the manner in which the wing is subdivided, each element or portion thereof lying in the region of integration S_o will be either a rectangle or triangle, as shown in Figure 16. The integral expression for a typical element is

$$\Delta w(x,y) = \frac{1}{4\pi} \int_{y_1}^{y_2} \int_{x_1}^{x_2} \frac{\Delta C_p(x_o,y_o)}{(y-y_o)^2} \cdot \frac{(x-x_o)\,dx_o\,dy_o}{\sqrt{(x-x_o)^2-\beta^2(y-y_o)^2}} \tag{75}$$

Note that for sufficiently small elements the pressure loading is essentially constant over the entire element. Consequently, it may be

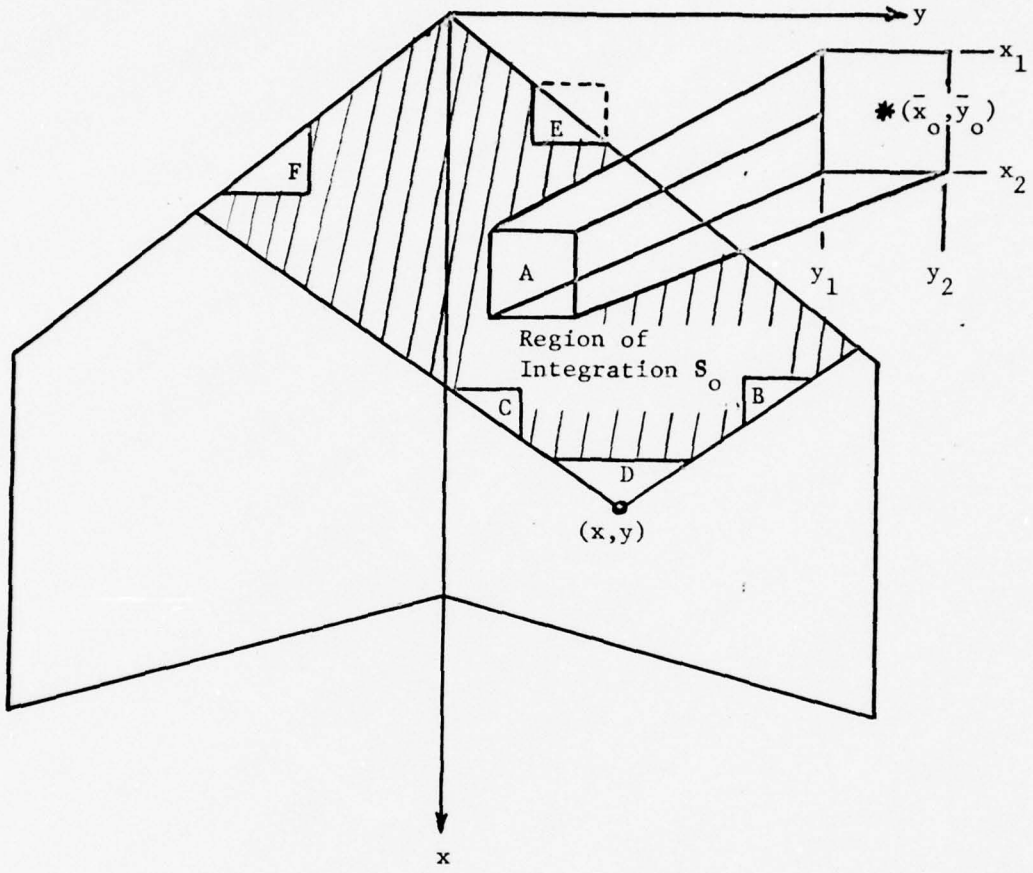


Figure 16. Element Shapes.

taken outside the integral and evaluated at the element centroid $(\bar{x}_o, \bar{y}_o)$ with the result

$$\Delta w(x,y) = \frac{\Delta C_p(\bar{x}_o, \bar{y}_o)}{4\pi} \int_{y_1}^{y_2} \int_{x_1}^{x_2} \frac{(x-x_o)\,dx_o\,dy_o}{(y-y_o)^2\sqrt{(x-x_o)^2-\beta^2(y-y_o)^2}} \tag{76}$$

The integral in Equation (76) may be evaluated in closed form when the appropriate limits of integration are known. For rectangular elements such as element A in Figure 16, the result is

$$\Delta w(x,y) = \frac{\beta \Delta C_p(\bar{x}_o, \bar{y}_o)}{4\pi} \left[-K(x_2,y_2) + K(x_2,y_1) + K(x_1,y_2) - K(x_1,y_1)\right] \tag{77}$$

where

$$K(x_o,y_o) = \frac{\sqrt{(x-x_o)^2 - \beta^2(y-y_o)^2}}{\beta(y-y_o)} + \text{Arctan}\left\{\frac{\beta(y-y_o)}{\sqrt{(x-x_o)^2 - \beta^2(y-y_o)^2}}\right\} \tag{78}$$

For triangular elements bounded by Mach lines, such as elements B and C, the lower x-limit is a function of y_o. The form of this function causes certain terms to vanish during the integration. Results for both elements B and C are then

$$\Delta w(x,y) = \frac{\beta \Delta C_p(\bar{x}_o, \bar{y}_o)}{4\pi} \left[K(x_1,y_2) - K(x_1,y_1)\right] \tag{79}$$

where the K-function is given by Equation (78). For element D, which includes the point (x,y) on its boundary, two separate integrals as well as the poles of two inverse-tangent functions must be evaluated. The integration and evaluation yields the well-known Ackeret result (Ref. 34) for an infinite span wing:

$$\Delta w(x,y) = - \frac{\beta \Delta C_p(\bar{x}_o, \bar{y}_o)}{4} \tag{80}$$

The exact integrals for elements cut by the wing leading edge, such as E and F, yield three complicated expressions, depending on whether the leading edge is subsonic, sonic, or supersonic. Rather than using the complicated results, the downwash due to these elements is approximated by using one-half of the value due to a rectangular element with the same x and y dimensions. The outlines of such elements are shown by dashed lines in Figure 16. The equations for the downwash is then one-half the value of Equation (77):

$$\Delta w(x,y) = \frac{\beta \Delta C_p(\bar{x}_o, \bar{y}_o)}{8\pi} \left[-K(x_2 y_2) + Kx_2 y_1) + K(x_2 y_1) + K(x_1 y_2) - K(x_1 y_1)\right] \tag{81}$$

The pressure loading $\Delta C_p(\bar{x}_o, \bar{y}_o)$ is evaluated at the centroid of the triangular element. This approximation would be expected to have little effect except for control points close to the leading edge of very highly swept wings.

The only remaining task is to evaluate the unknown coefficients B_{nm} in the pressure loading Equation (54). This requires introducing the tangency condition

$$\sin \alpha(x,y) + w(x,y) = 0 \tag{82}$$

where $\sin \alpha(x,y)$ is the freestream velocity component normal to the wing at (x,y). Equation (82) is the expression for no flow through the wing surface and must be satisfied at every control point on the wing. Using the previously developed equations leads to

$$\int_{S_o}\int \Delta C_p(\bar{x}_o,\bar{y}_o)\ K_o(x,y,x_1,y_1,x_2,y_2) = -\frac{4\pi}{\beta}\sin\alpha(x,y) \tag{83}$$

where K_o is the appropriate K-function from Equations (77) through (81) (Note that $K_o = -\pi$ for Equation (80). When the pressure loading formula Equation (54) is inserted into Equation (83), there are (N+1)x(M+1) unknowns B_{nm} in the resulting eqpression. Choosing spanwise and chordwise control points according to

$$y_m = \frac{1}{2}\left[1 - \cos\left\{\frac{\pi(m+1)}{M+2}\right\}\right],\ m=0,1,\ldots,M \tag{84}$$

$$x_j = x_{LE}(y_m) + \frac{1}{2}\,c(y_m)\left[1 - \cos\left\{\frac{\pi(n+1)}{N+1}\right\}\right],\ n=0,1,\ldots,N \qquad j=n+mN \tag{85}$$

and evaluating Equation (83) at each control point will give a complete set of algebraic equations, one for each unknown coefficient B_{nm}. Inserting the pressure formula Equation (54), this set may be arranged in the matrix form

$$[a_{ij}]\{b_j\} = -\frac{4\pi}{\beta}\{\sin\alpha(x_j,y_m)\} \tag{86}$$

where

$$a_{ij} = \int_{S_o}\int P(\bar{x}_o\bar{y}_o)\bar{\xi}^n \sin\{(m+1)\bar{\theta}\}\ K_o(x_j,y_m,x_1,y_1,x_2,y_2) \tag{87}$$

and b_j is the column vector of unknown coefficients B_{nm} where $j = n+mN$. Inversion of the system is accomplished with a Gaussian elimination algorithm.

Once the B_{nm} coefficients have been obtained, the value of the pressure loading is known at every point on the wing surface. Values of section and total loads and corresponding moments may then be obtained using the standard aerodynamic formulas (Ref. 34) and numerical quadrature.

Results

Before attempting to calculate loads on a warped wing in the presence of a body, it was felt that a numerical study was necessary to test the validity and accuracy of the basic method. This study investigated the effects of: (1) number of and placement of control points; (2) discretization of the lifting surface; (3) panel size; (4) polynomial forms; (5) leading edge element approximation; and (6) flow tangency.

The best test for the method is, of course, comparison with experiment. For this purpose, two low aspect ratio wings were chosen, one delta and one trapezoidal. Planform schematics and (NC=6)x(NS=6) control point grids for each wing are shown in Figure 17. Theoretical distributions of pressure loading coefficient ΔC_p were compared with experimental results (from Reference 42) at 6° angle of attack and two Mach numbers, 1.61 and 2.01.

Some representative results for each wing are shown in Figures 18 through 21. These results are intended to show that the supersonic weighting function is valid and that the general method of solution has good agreement with theory, even for the highly swept delta wing. General results and some of the problems encountered with each wing will be discussed separately.

The first example in Figures 18 and 19 is the aspect ratio 1.342 trapezoidal wing. The wing has a 25° leading edge sweep and a taper

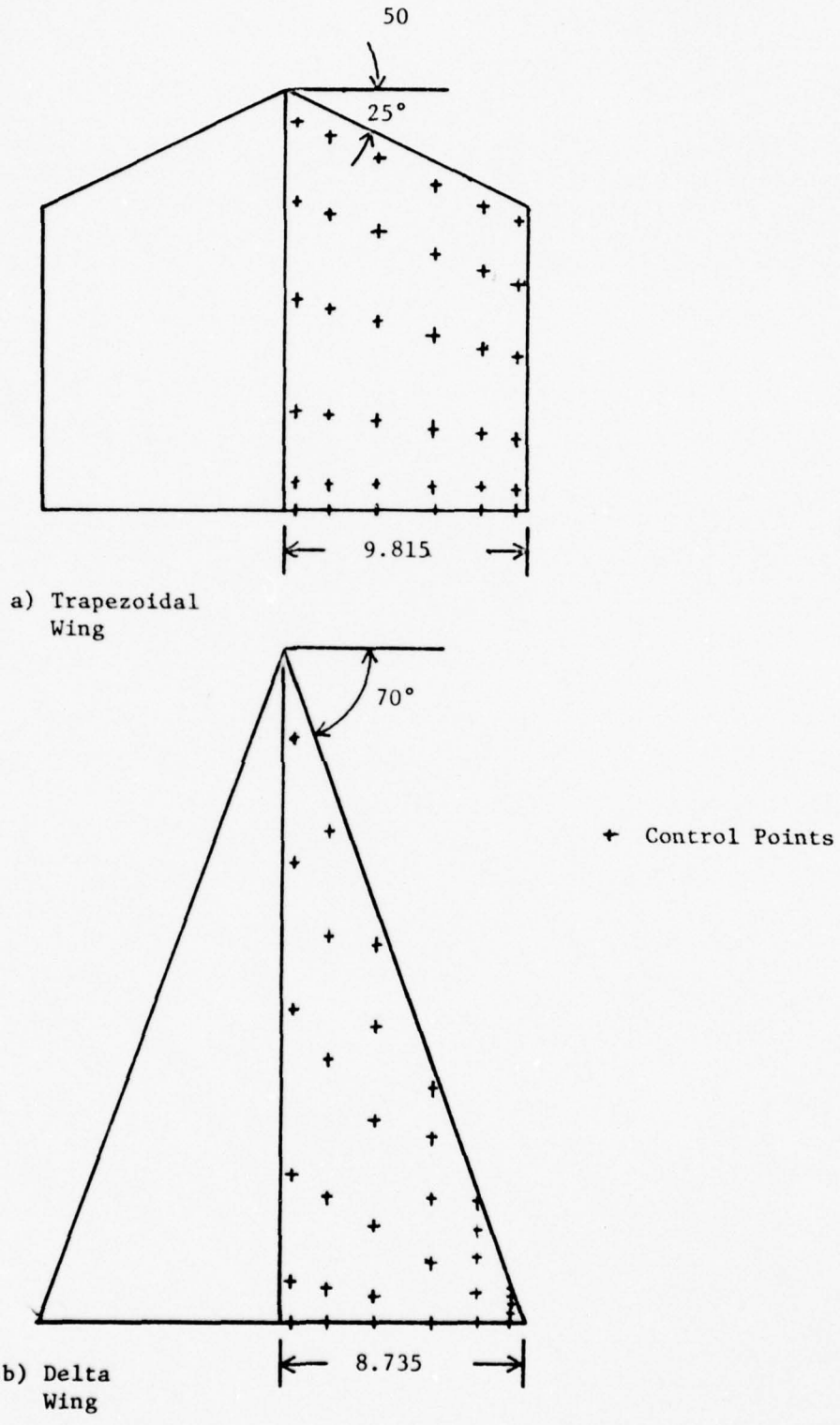


Figure 17. Control Point Location on Two Wings in Supersonic Flow (Ref. 42).

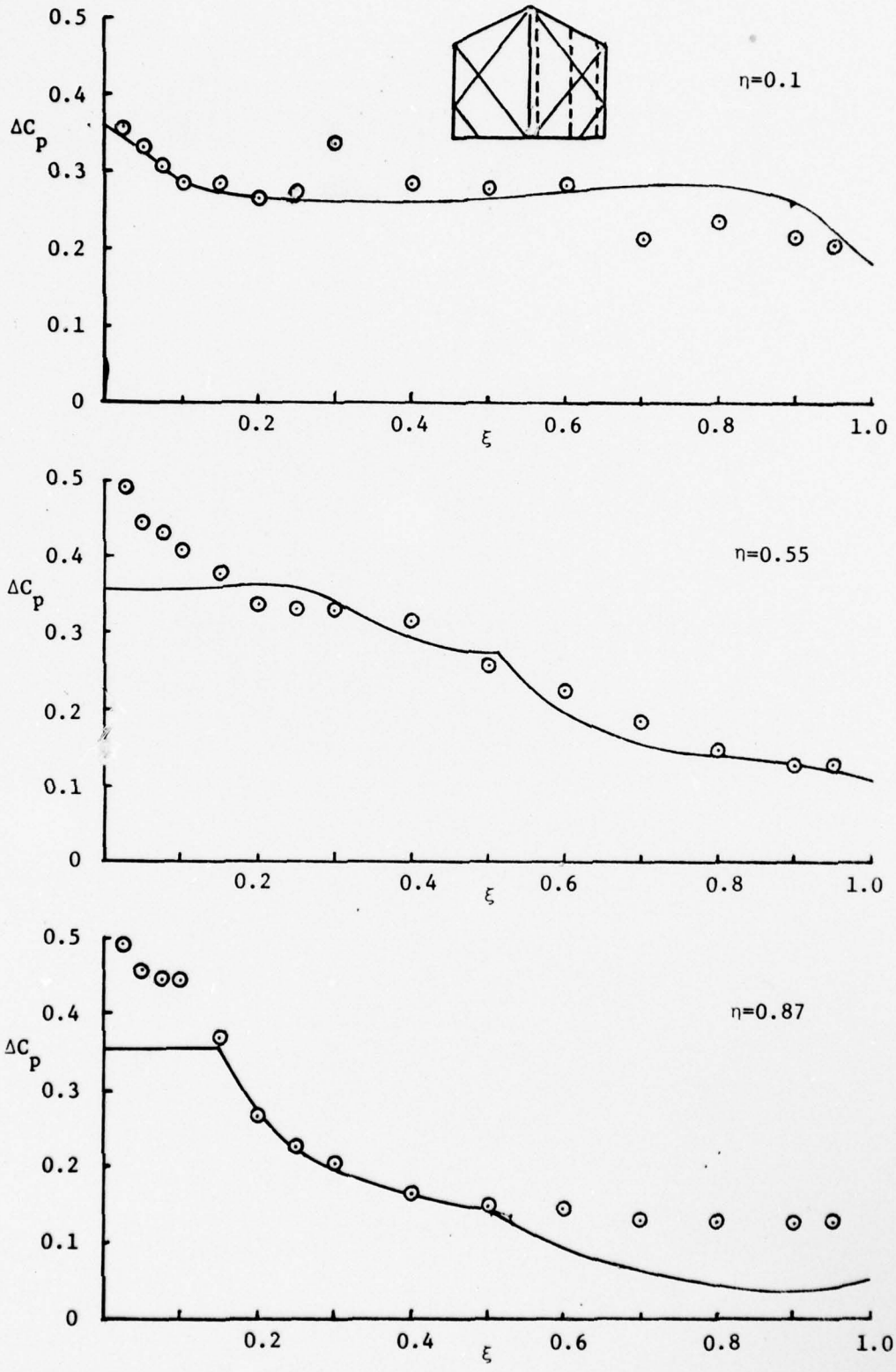


Figure 18. Chordwise Pressure Distribution on a Trapezoidal Wing in Supersonic Flow (M=1.61).

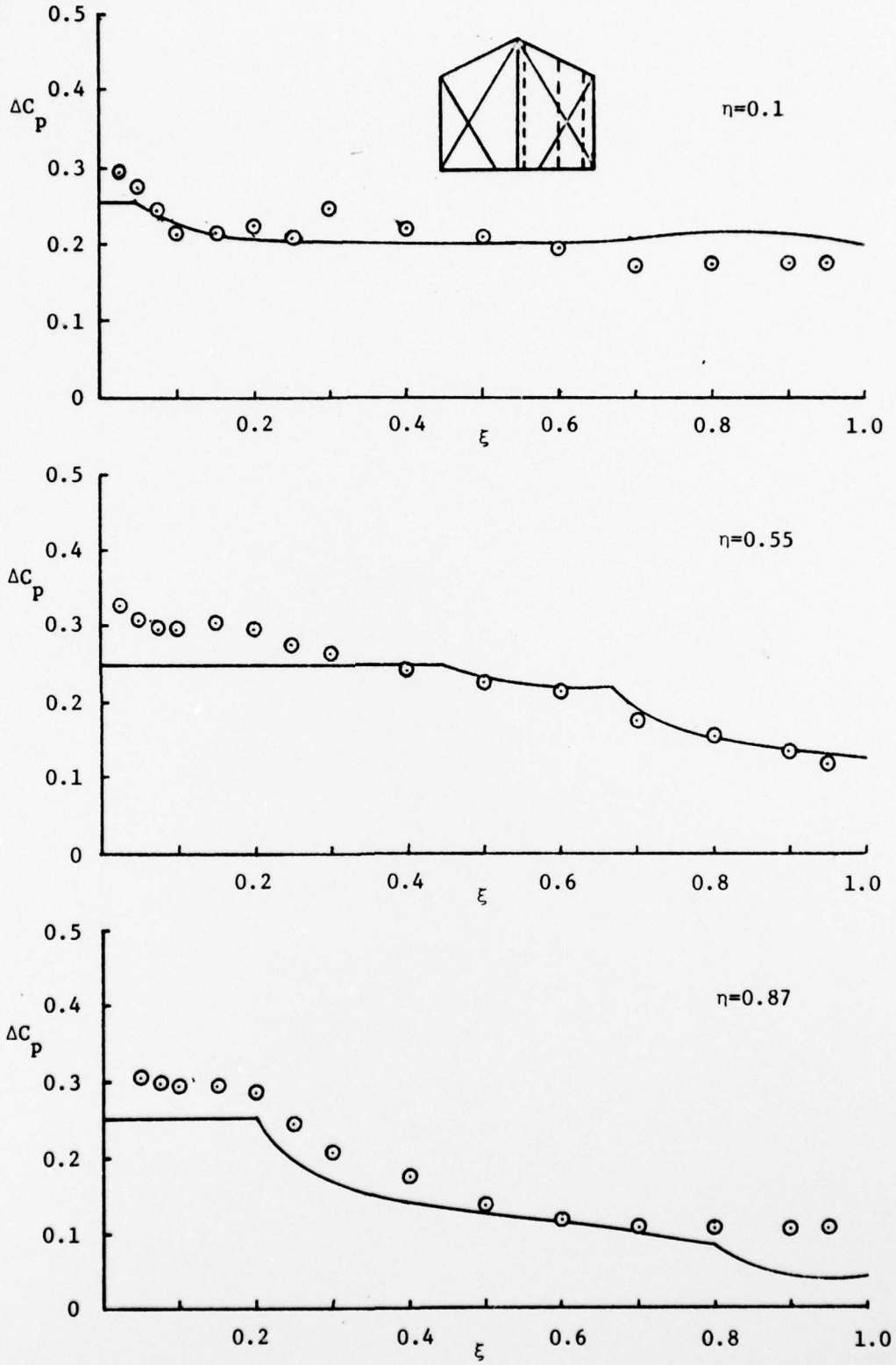


Figure 19. Chordwise Pressure Distribution on a Trapezoidal Wing in Supersonic Flow (M=2.01).

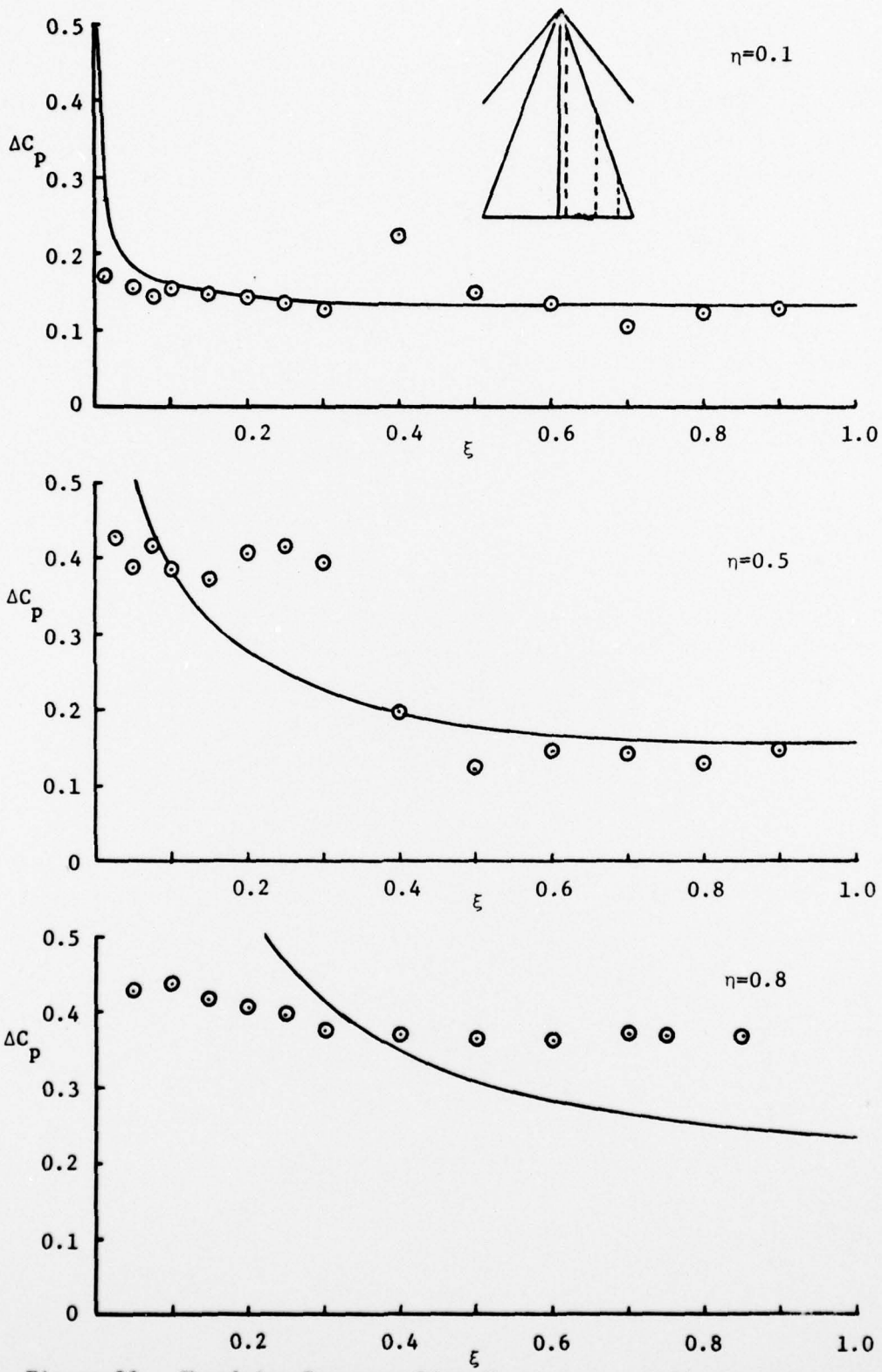


Figure 20. Chordwise Pressure Distribution on a Delta Wing in Supersonic Flow (M=1.61).

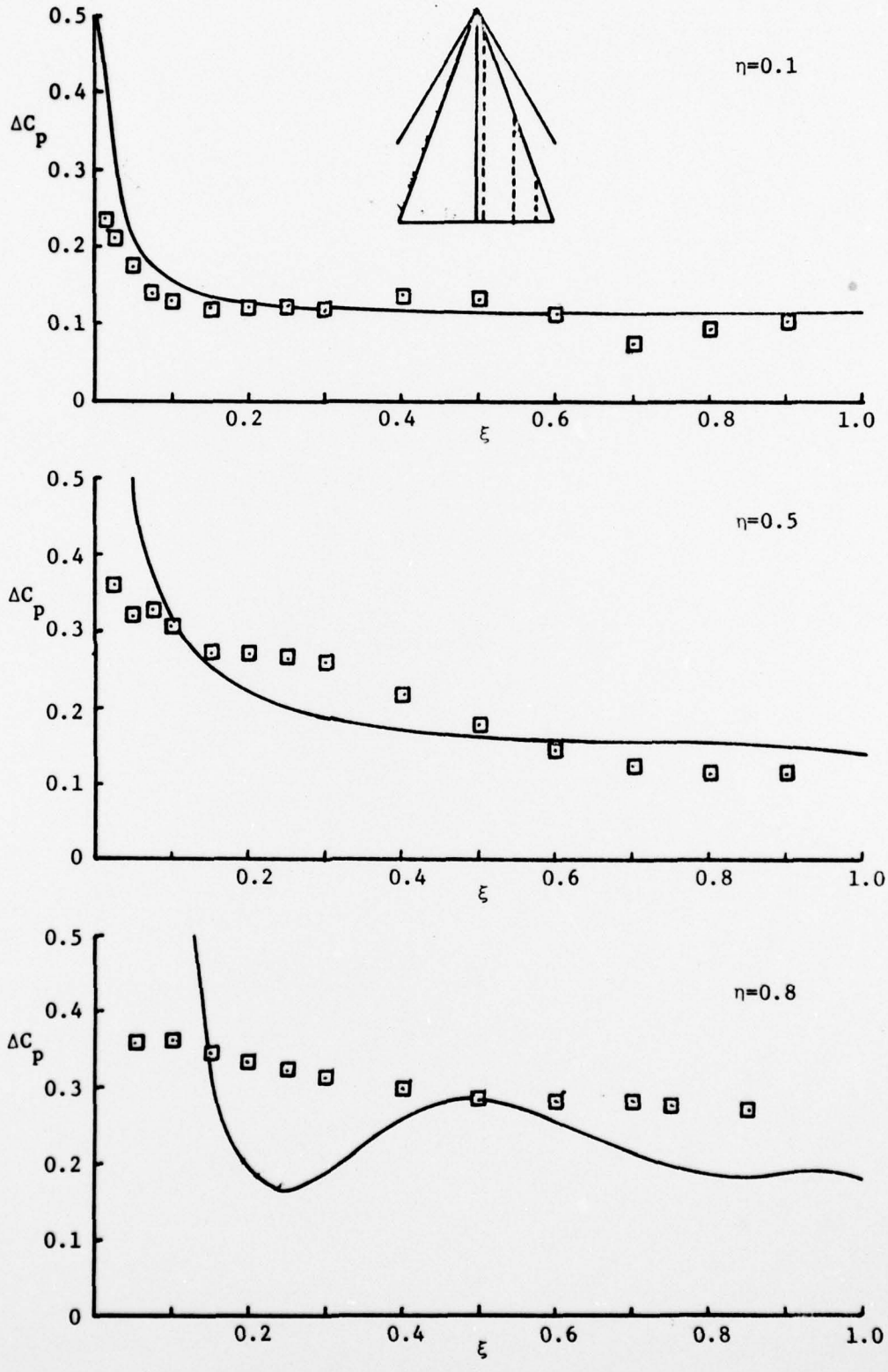


Figure 21. Chordwise Pressure Distribution on a Delta Wing in Supersonic Flow (M=2.01).

ratio of 0.721. The airfoil section is a 3% circular arc, which is essentially a zero-thickness wing and ideally suited to the present theory. The leading edge is supersonic for both Mach numbers shown. The (NC=6)x(NS=6) control point grid shown in Figure 17 was used to obtain the results shown. The wing was divided into 100 evenly spaced spanwise panels with 45 chordwise panels. The chordwise panel spacing used the cosine distribution which placed smaller panels near the leading and trailing edges. Results agree exceptionally well with experiment except over the rear half of the chord at the η=0.97 spanwise location. The disagreement in this region is probably due to viscous effects.

Figures 20 and 21 present results for the aspect ratio 1.456 delta wing. The wing has a 70° leading edge sweep, which is subsonic for both Mach numbers 1.61 and 2.01. The chordwise airfoil section is a NACA 65A003 thickness distribution, which is a 3% thick symmetric airfoil with a rounded leading edge. The (NC=6)x(NS=6) control point grid shown in Figure 17 was used to obtain all results shown for this wing. Overall agreement between theory and experiment is quite good, the major disagreement occurring in the expected places - near the blunt leading edge and at the extreme wing tip.

During the development of the numerical method several equations presented in the theory section had to be modified to obtain acceptable results for the delta wing. The assumed pressure loading form used for the delta wing is

$$\Delta C_p(x_o,y_o) = P(x_o,y_o) \sum_{n=0}^{N} \sum_{m=0}^{M} B_{nm}\, \eta^m \cos\left(\frac{n\pi\xi}{2}\right) \qquad (88)$$

which replaced Equation (54). A cosine distribution, rather than even spacing, was used for the spanwise panel size. Smaller panels were placed near the wing tip. The control point placement along a chord was

$$x_j = x_{LE}(y_m) + \frac{1}{2}\, c(y_m) \cos\left\{\frac{\pi(N-n)}{N+1}\right\}, \quad \begin{matrix} n=0,1,\ldots,N \\ j=n+mN \end{matrix} \tag{89}$$

which replaced Equation (85). Numerical studies have subsequently shown that these changes were required because the region of integration, or forecone, for control points near the leading edge was not subdivided finely enough. This subdivision is particularly critical for highly swept wings with subsonic leading edges.

Numerical tests were also made using various numbers of spanwise and chordwise panels and various control point combinations. Acceptable results could be produced with a coarser control point grid, such as (NC=3)x(NS=4), and in some cases the comparison with experiment was slightly better than that shown in Figures 18 through 21. The (NC=6)x(NC=6) results were shown in the current report for two reasons. First, it is anticipated that for a warped wing a large number of control points will be needed to accurately define the pressure field. Second, some classical lifting surface methods have yielded divergent results when increasing numbers of control points were used. The present method has not exhibited such trends, even for (NC=6)x(NS=8) grids. Typical computation times were 45 seconds for the (3x4) case and 118 seconds for the (6x6) case on an IBM 370/155.

Conclusions

The original intent during development of the supersonic program was to use the existing subsonic program and make the two almost identical -

the only mofifications being the closed form Kernel integrals and the limiting region of integration for a control point from the entire wing to the forecone. It was felt that this approach would require minimal effort and allow rapid development of the supersonic method. Such was not to be the case, however.

It became immediately apparent that different weighting functions were required for the assumed pressure loading, and considerable time was required to develop these from the exact forms given in the literature (Refs. 40, 41, 43). However, as Cunningham discovered (Ref. 32), results using these functions were far superior to those using the subsonic program forms.

Several other conclusions which need to be noted were reached during the numerical study of the basic supersonic method. In the current version, the placement of control points must vary depending on whether the leading edge is subsonic or supersonic. The area of integration for each control point needs to be subdivided better, particularly for control points near the leading edge. The latter change may allow standardization of control point placement, and may also minimize the effects of the leading edge element approximation, even on highly swept-wings. A new form for the assumed polynomial distribution is indicated. This new form should be applicable to wings of any taper ratio. This need may become even more apparent when body effects and wing warpage are included.

Finally, planar wing results using the method in its current form show good agreement with experiment and are not divergent with increasing numbers of control points. It is felt, however, that any or all of the previously mentioned changes could noticeably improve the results and

possibly the convergence of the method. It would also be desirable if results and computation requirements could be compared with other numerical methods such as References 31, 7, or 32.

REFERENCES

1. Smith, A. M. O., and Pierce, J., "Exact Solution of the Neumann Problem. Calculation of Non-Circulatory Plane and Axially Symmetric Flow About or Within Arbitrary Boundaries," Douglass Aircraft Company, Report ES 26988, August 1958.

2. Blackwell, J. A., "A Finite Step Method for Calculation of Theoretical Load Distributions for Arbitrary Lifting Surface Arrangements at Subsonic Speeds," NASA TN D-5335, July 1969.

3. Mook, D. T., and Maddox, S. A., "Extension of a Vortex-Lattice Method to Include the Effects of Leading Edge Separation," AIAA Journal of Aircraft, February 1974, Vol. 11, No. 2.

4. Kalman, T. P., Rodden, W. P., and Geising, J. P., "Application of the Doublet-Lattice Method to Non-Planar Configurations in Subsonic Flow," AIAA Journal of Aircraft, June 1971, Vol. 8, No. 6.

5. Bradley, R. G., and Miller, B. D., "Application of Finite Element Theory to Airplane Configurations," AIAA Journal of Aircraft, June 1971, Vol. 8, No. 6.

6. Geising, J. P., "Lifting Surface Theory for Wing-Fuselage Combinations," Report DAC-67212, McDonnel-Douglass Aircraft Corporation, August 1968.

7. Woodward, F. A., "Analysis and Design of Wing-Body Combinations at Subsonic and Supersonic Speeds," AIAA Journal of Aircraft, Nov-Dec 1968, Vol. 5, No. 6.

8. Hua, H. M., "A Finite-Element Method for Calculating Aerodynamic Coefficients of a Subsonic Airplane," AIAA Journal of Aircraft, July 1973, Vol. 10, No. 7.

9. Rodden, W. P., Geising, J. P., and Kalman, T. P., "Refinement of the Non-Planar Aspects of the Subsonic Doublet-Lattice Lifting Surface Method," AIAA Journal of Aircraft, January 1972, Vol. 9, No. 1.

10. South, J. C., and Jameson, A., "Relaxation Solutions for Inviscid Axisymmetric Transonic Flow Over Blunt or Pointed Bodies," Proceedings: AIAA Computational Fluid Dynamics Conference, July 1973.

11. Jameson, A., "Numerical Calculation of the Three-Dimensional Transonic Flow Over a Yawed Wing," Proceedings: AIAA Computational Fluid Dynamics Conference, July 1963.

12. Klunker, E. B., and Newman, P. A., "Computation of Transonic Flow about Lifting Wing-Cylinder Combinations," AIAA Journal of Aircraft, April 1974, Vol. 11, No. 4.

13. Nielsen, J. N., Kaatari, G. E., and Anastosio, R. F., "A Method for Calculating the Lift and Center of Pressure of Wing-Body-Tail Combinations at Subsonic, Transonic and Supersonic Speeds," NACA RM A53G08, November 1953.

14. Howard, M. L., Brooks, E. N., and Saffel, B. F., "A Method for Predicting the Static Aerodynamic Characteristics of Typical Missile Configurations for Angles of Attack to 180 Degrees," NSRDC Report 3645, 1971.

15. Moore, F. G., "Aerodynamics of Guided and Unguided Weapons," NWL TR-3018, December 1973.

16. Douglass Aircraft Co., Inc., "USAF Stability and Control DATCOM," Revisions by Wright-Patterson AFB, July 1963.

17. Rossow, V. J., "Conformal Mapping for Potential Flow About Airfoils with Attached Flap," AIAA Journal of Aircraft, January 1973, Vol. 10, No. 1.

18. Foster, D. N., "Flow Around Wing Sections with High Lift Devices," AIAA Journal of Aircraft, March 1972, Vol. 9, No. 3.

19. Cunningham, A. M., "Oscillatory Supersonic Kernel Function Method for Interfering Surfaces," AIAA Journal of Aircraft, November 1974, Vol. 11, No. 11.

20. Cunningham, A. M., "Unsteady Subsonic Collocation Method for Wings With and Without Control Surfaces," AIAA Journal of Aircraft, June 1972, Vol. 9, No. 6.

21. Purvis, J. W., "Simplified Solution of the Compressible Subsonic Lifting Surface Problem," Master's Thesis, Aerospace Engineering Department, Auburn University, August 1975.

22. Chadwick, W. R., "The Application of Non-Planar Lifting Surface Theory to the Calculation of External Store Loads," NWL TR-2696, November 1971.

23. Ashley, H., Widnall, S., and Landahl, M., "New Directions in Lifting Surface Theory," AIAA Journal, January 1965, Vol. 3, No. 1.

24. Rowe, W. S., Winther, B. A., and Redman, M. C., "Unsteady Subsonic Aerodynamic Loadings Caused by Control Surface Motions," AIAA Journal of Aircraft, January 1974, Vol. 11, No. 1.

25. Lamar, J. E., "Extension of Leading-Edge-Suction Analogy to Wings with Separated Flow Around the Side Edges at Subsonic Speeds," NASA TR R-428, October 1974.

26. Gersten, K., "A Non-Linear Lifting Surface Theory Especially for Low Aspect Ratio Wings," AIAA Journal, April 1963.

27. Walkley, K. B., and Martin, F. W., "Aerodynamic Interference of Wing-Pylon-Body Combinations at Low Subsonic Speeds," Air Force Armament Laboratory, Technical Report AFATL-TR-73-162, August 1963.

28. Evvard, J. C., "Use of Source Distributions for Evaluating Theoretical Aerodynamics of Thin Finite Wings at Supersonic Speeds," NACA TR-951, 1950.

29. Etkin, B. E., and Woodward, F. A., "Lift Distributions on Supersonic Wings with Subsonic Leading Edges and Arbitrary Angle-of-Attack Distribution," Second Canadian Symposium on Aerodynamics, University of Toronto.

30. Purvis, J. W., "Airload Distribution on Damaged Supersonic Wings," NWL TR-3178, August 1974.

31. Carlson, H. W., and Miller, D. S., "Numerical Methods for the Design and Analysis of Wings at Supersonic Speeds," NASA TN D-7713, December 1974.

32. Cunningham, A. M., "Oscillatory Supersonic Kernel Function Method for Isolated Wings," AIAA Journal of Aircraft, Pctpber ;974, Vol. 11, No. 10.

33. Spratley, A. V., "Theoretical Pressure Distribution Over an Arbitrary Body of Revolution at an Angle-of-Attack in Supersonic Flow," Master's Thesis, Aerospace Engineering Dpeartment, Auburn University, March 1975.

34. Ashley, H., and Landahl, M., Aerodynamics of Wings and Bodies, Addison-Wesley, 1965.

35. Spangler, S. B., Goodwin, F. K., and Nielsen, J. N., "Analytical Investigation of Hinge Moments on Missile Trailing-Edge Control Surfaces," Nielsen Engineering and Research, Inc., September 1974.

36. Burkhalter, J. E., "Aerodynamic Analysis of Highly Deformed Wing Body Combination in Subsonic and Supersonic Flow," Proposal Submitted to U.S. Army Research Office, January 1976.

37. Shelton, Michael S., "An Analytical Investigation of the Thick Airfoil Problem Using Vortex-Paneling," Paper Presentation, AIAA Southeast Regional Student Conference, April 1977.

38. Wick, Bradford H., "Chordwise and Spanwise Loadings Measured at Low Speed on a Triangular Wing Having an Aspect Ratio of Two and an NACA 0012 Airfoil Section," NACA TN 1650, June 1948.

39. Glauert, H., "A Theory of Thin Airfoils," Aeronautical Research Committee, Reports and Memorandum 910, London, 1924.

40. Malvestuto, F. S., Margolis, K., and Ribner, H. S., "Theoretical Lift and Damping in Roll of Thin Sweptback Wings of Arbitrary Taper and Sweep at Supersonic Speeds - Subsonic Leading Edges and Supersonic Trailing Edges," NACA TN 1860, 1949.

41. Harmon, S. M., and Jeffreys, I., "Theoretical Lift and Damping in Roll of Thin Wings with Arbitrary Sweep and Taper at Supersonic Speeds - Supersonic Leading and Trailing Edges," NACA TN 2114, 1950.

42. Landrum, E. J., "A Tabulation of Wind-Tunnel Pressure Data and Section Aerodynamic Characteristics at Mach Numbers of 1.61 and 2.01 for Two Trapezoidal and Three Delta Wings Having Different Surface Shapes," NASA TN D-1394, 1962.

43. Cohen, D., "Formulas for the Supersonic Loading, Lift and Drag of Flat Sweep-Back Wings with Leading Edges Behind the Mach Lines," NACA Report 1050, 1951.

44. Pitts, W. C., Nielson, J. N., and Kaattai, G. E., "Lift and Center of Pressure of Wing-Body-Tail Combinations at Subsonic, Transonic, and Supersonic Speeds," NACA TR-13-7, 1957.

45. Martin, J. C., and Jeffreys, I., "Span Load Distributions Resulting from Angle-of-Attack, Rolling, and Pitching for Tapered Sweptback Wings with Streamwise Tips," NACA TN-264B, 1952.

46. Etkin, B. E., and Woodward, F. A., "Lift Distributions on Supersonic Wings with Subsonic Leading Edges and Arbitrary Angle-of-Attack Distribution," Second Canadian Symposium on Aerodynamics, University of Toronto, 1965.

47. Purvis, J. W., "Airload Distribution on Damaged Supersonic Wings," U.S. Naval Weapons Laboratory, TWL TR-3178, 1974.

48. Pines, S., Dugundji, J., and Neuringer, J., "Aerodynamic Flutter Derivatives for a Flexible Wing with Supersonic and Subsonic Edges," Journal of the Aerospace Sciences, Vol. 22, No. 10, 1955.

49. Appa, K., and Smith, G. C. C., "Finite Element Approach to the Integrated Formulation of General Unsteady Supersonic Aerodynamics," NASA CR-2296, 1973.

50. Curtis, A. R., and Lingard, R. W., "Unsteady Aerodynamic Distributions for Harmonically Deforming Wings in Supersonic Flow," AIAA Paper 68-74, January, 1968.

51. Miranda, Luis R., "Extended Applications of the Vortex Lattice Method," Vortex Lattice Utilization, NASA SP-405, 1976.

52. Carlson, H. W., and Middleton, W. D., "A Numerical Method for the Design of Camber Surfaces of Supersonic Wings with Arbitrary Planforms," NASA TN D-2341, 1964.

53. Middleton, W. D., and Lundry, J. L., "A Computational System for Aerodynamic Design and Analysis of Supersonic Aircraft; Part 1 - General Description of Theoretical Development," NASA CR-2715, 1976.

APPENDIX

DERIVATION OF THE COMPRESSIBLE LIFTING SURFACE POTENTIAL

The following derivation parallels that given in Reference 3 for incompressible flow, which begins with the most elementary solution of the linearized potential equation, the point source. The potential for a point source in compressible flow is

$$\phi^S = -\frac{m}{4\pi r} \tag{A-1}$$

where m is the source strength, r is the elliptic radius defined by

$$r = \sqrt{x^2 + \beta^2 y^2 + \beta^2 z^2} \tag{A-2}$$

and the Mach parameter β is $\sqrt{1-M^2}$.

The potential for a doublet with its axis oriented in the z-direction is found by differentiating (A-1) with respect to z:

$$\phi^D = \frac{\partial \phi^S}{\partial z} = \frac{m\beta^2 z}{4\pi r^3} \tag{A-3}$$

The solution for the elemental horseshoe vortex is the integral of a semi-infinite line of doublets:

$$\phi^\Gamma = \int_0^\infty \phi^D \, dz_o = \frac{m\beta^2 z}{4\pi} \int_0^\infty \frac{dx_o}{[(x-x_o)^2 + \beta^2 y^2 + \beta^2 z^2]^{3/2}} \tag{A-4}$$

Performing the integration and evaluating the limits gives:

$$\phi^\Gamma = \frac{mz}{4\pi(y^2+z^2)} \left[1 + \frac{x}{\sqrt{x^2+\beta^2 y^2+\beta^2 z^2}} \right] \tag{A-5}$$

which differs from the incompressible results only by the β^2 terms in the radical.

Now consider a sheet of these elemental vortices, lying in the z=0 plane. The constant m is replaced by $\gamma(x_o,y_o)$ the vorticity per unit area, which is assumed to be a function of the position on the surface. The potential at any arbitrary point (x,y,z) in the flow field due to an infinitesimal area $dx_o dy_o$ of the sheet is

$$d\phi(x,y,z) = \frac{1}{4\pi} \frac{\gamma(x_o,y_o)}{(y-y_o)^2+z^2} \; z \left[1 + \frac{(x-x_o)}{\sqrt{(x-x_o)^2+\beta^2(y-y_o)^2+\beta^2 z^2}} \right] dx_o dy_o \quad \text{(A-6)}$$

Denoting the total surface area of the sheet by S, the potential due to the entire surface is then

$$\phi(x,y,z) = \iint_S d\phi(x,y,z) \quad \text{(A-7)}$$

or

$$\phi(x,y,z) = \frac{1}{4\pi} \iint_S \frac{\gamma(x_o,y_o)}{(y-y_o)^2+z^2} \; z \left[1 + \frac{(x-x_o)}{\sqrt{(x-x_o)^2+\beta^2(y-y_o)^2+\beta^2 z^2}} \right] dx_o dy_o \quad \text{(A-8)}$$

For supersonic flow, the result is

$$\phi(x,y,z) = \frac{1}{2\pi} \iint_{S_o} \frac{\gamma(x_o,y_o)}{(y-y_o)^2+z^2} \cdot \frac{z\,(x-x_o)}{\sqrt{(x-x_o)^2-\beta^2(y-y_o)^2-\beta^2 z^2}} \, dx_o dy_o \quad \text{(A-9)}$$